EFFECTS OF TIRE ATTRIBUTES ON THE AERODYNAMIC PERFORMANCE OF A REALISITIC CAR-TIRE ASSEMBLY AND THE SENSITIVITY ANALYSIS TO UNDERSTAND THE IMPACT OF THE RIM PROTECTOR

Shubham Rath

Thesis submitted to the faculty of the Virginia Polytechnic Institute and State University in partial fulfillment of the requirements for the degree of

Master of Science

In

Mechanical Engineering

Alexandrina Untaroiu, Chair

Juliana P. Duarte

Saad A. Ragab

11th May 2022

Blacksburg, Virginia

Keywords: CFD, Tire Research, Computational Modelling, Numerical Analysis

EFFECTS OF TIRE ATTRIBUTES ON THE AERODYNAMIC PERFORMANCE OF A REALISITIC CAR-TIRE ASSEMBLY AND THE SENSITIVITY ANALYSIS TO UNDERSTAND THE IMPACT OF THE RIM PROTECTOR

Shubham Rath

ABSTRACT

The effect that the tire has on the overall aerodynamic drag in a car-tire assembly has been studied and deemed considerable from past studies. It has been shown that to know how tire parameters affect the drag on the car-tire assembly, it is important to understand how the vehicle body and the tires influence the flow structures. Previous studies have focused on the tire attributes that have some impact on the aerodynamic performance of the vehicle. These tire attributes, however, haven't been studied to the extent where one can get a better understanding of the impact of each of these attributes. This paper studies the impact that specific tire attributes have on the overall aerodynamic drag on the vehicle based on a thorough and systematic sensitivity study. The effect of tire attributes in a vehicle assembly as well as the sensitivity study of a rim protector on a standalone tire is conducted. This helps in better understanding the flow structures around the car body and around the tire for the improvement in the aerodynamic performance of the vehicle.

This is a two-part study. One component of this study is a parametric sensitivity analysis of a tire in a tire – vehicle assembly. The other component is a parametric sensitivity analysis of the rim protector design on a standalone tire.

EFFECTS OF TIRE ATTRIBUTES ON THE AERODYNAMIC PERFORMANCE OF A REALISITIC CAR-TIRE ASSEMBLY AND THE SENSITIVITY ANALYSIS TO UNDERSTAND THE IMPACT OF THE RIM PROTECTOR

Shubham Rath

GENERAL AUDIENCE ABSTRACT

The drag performance is one of the most important factors that contributes to the overall efficiency of a vehicle. There has always been a huge demand in the automotive industry for such studies. Over the years, experimental studies conducted have shown to be invaluable to the industry. But a big downside to experimental studies is that they are extremely expensive. Experimental studies on Vehicle bodies require a wind tunnel and expensive measurement equipment. This has led to a high demand for more computational studies in this field. Various authors over the past few years have studied and challenged various solution procedures used in computational studies. The trade-off for these studies is always cost vs. accuracy. This thesis attempts to simulate both for a vehicle assembly as well as a standalone tire model to come up with a robust solution method for the computational analysis of flow over a vehicle body. The goal of this thesis is to conduct a parametric sensitivity study for the cross-section profile of the tire in vehicle assembly as well as a parametric sensitivity study for the rim protector profile of the tire in a standalone tire.

At the end of the study, we will get a better understanding of the impact that each of the parameters have on the drag performance of the vehicle and the standalone tire.

Dedication

My Parents for supporting me through all the difficult times during the Pandemic.

Acknowledgement

I would like to thank my advisor Dr. Alexandrina Untaroiu for her support and help through Graduate School. Her contributions to the research I've conducted here at Virginia Tech have been immense. Gen Fu's contribution to the project have also been invaluable since he started working on this project before I took over since he graduated with a Ph.D. from Virginia Tech. Gen's previous work has been a great source of insight for the content discussed in this thesis.

I would also like to express my gratitude for the support and guidance from the CenTiRe industry mentors. This work was funded by the NSF through the IUCRC/CenTiRe research center at Virginia Tech.

Finally, I would like to thank Dr. Saad Ragab and Dr. Juliana Pacheco Duarte for agreeing to serve on my Defense committee.

Table of Contents

Contents

List of Figures

List of Tables

Chapter 1: Introduction

1.1 Introduction

Investigating the drag contribution of vehicle components is one of the most imperative tasks in order to improve the fuel efficiency of vehicles. Tires contribute to about 25 percent of the overall vehicle drag [1]. This makes tire optimization for drag performance improvement extremely important for the automotive industry. Multiple studies have helped uncover the various techniques required to conduct aerodynamic analysis on tires as well as vehicle – tire assemblies [2-16, 22, 23]. These studies have highlighted the cost of conducting such analysis as well as the validity of the several techniques investigated. Due to the complex nature of conducting an aerodynamic analysis on tires or tire – vehicle assemblies, both the adequacy of the methods used as well as the cost of analysis are considered and challenged. The use of experimental techniques such as wind tunnel studies would be extremely expensive, and the resources required would be hard to come across. So, it was clear that a computational fluid dynamics study is the most effective way to conduct these studies.

Previous publications have discussed and shown the effectiveness of computational studies to conduct aerodynamic analysis of flow structures around vehicles and tires in terms of the accuracy of results [2-16, 22, 23]. The main goal of this study is to come up with a robust model for solving flow around both a standalone tire and a tire – vehicle assembly and to further understand the drag contribution of the tire. A preliminary study for optimizing the drag performance of the tire is done through a parametric sensitivity study of the tire. This is conducted for a validated tire-vehicle assembly model to determine the impact rank of certain tire parameters based on their sensitivity to drag area. These parameters are based on the cross-sectional geometry of the tire as well as the rim protector design of the tire

1.1.1 Motivation

There is an ever-increasing demand for more cost – effective techniques in order to conduct aerodynamic analysis in the automotive industry. Thus, it has become increasingly important to take steps in that direction. One such technique that explores more time and cost-effective ways to conduct aerodynamic analysis on vehicles is the usage of computational software in order to conduct such studies. The numerical solvers within these computational codes can, however, be inaccurate.

This comes as a cost of the usage of simplified models since unsteady turbulent flows don't have an exact solution. However, there have been numerous studies conducted in the past few years that have highlighted the accuracy of such models and this study tries to explore the same. Another demand within the automotive industry is understanding and optimizing the Drag performance of the tire. There are little to no studies that have explored the process of optimization of the drag performance of the tire through a parametric analysis in order to determine the impact of certain geometric parameters of the tire. To add to this discussion in a meaningful capacity, this thesis aims at conducting computational parametric studies for a validated tire-vehicle assembly model

1.1.2 Outline

This thesis is organized in order to navigate through the methodology, the findings and the discussions regarding the sensitivity study of the sidewall profile of the tire in a vehicle assembly and the sensitivity study of the rim protector profile. Chapter 2 introduces the design and methodology for the tire – vehicle assembly. This includes the geometry of the assembly, the mesh development, the proposed solution method as well as the parametrization of the tire. Chapter 3 then goes through the geometry of the standalone tire, the solution methodology as well as the parametrization of the rim protector. This then culminates into Chapter 4 where findings from the Design of experiments sensitivity study based on the solution methodology and the parameterization of the sidewall profile of the tire as well as the rim protector design are then discussed.

1.2 Literature Review

1.2.1 Vehicle Model

Over the years, computational studies on various vehicle models have been conducted some of the models used in those simulations were the Ahmed body and the SAE model as shown in Figure 1-1 [2]. These models are approximations of the overall geometry of the vehicle body and simplify some very important features such as mirrors, doorhandles, windshield, etc. of the vehicle body that have major contributions to the vehicle's drag contributions.

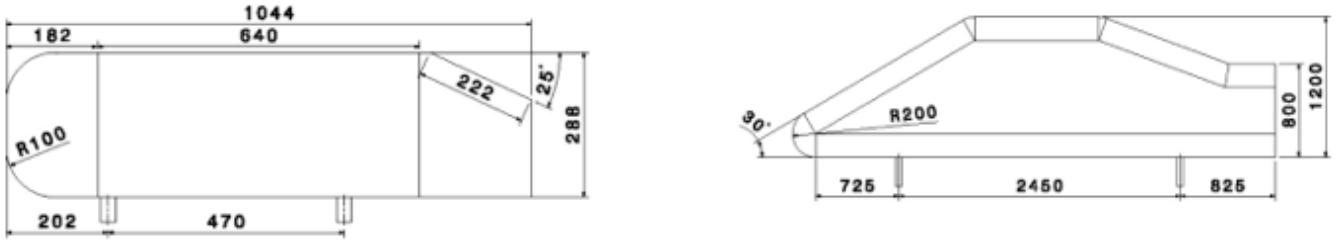

Figure 1-1: Ahmed Body (left) and SAE model (right) [2]

To conduct a thorough computational study on the aerodynamic phenomenon around the vehicle, the DrivAer model is selected. The DrivAer model, introduced by Heft *et al.* [2], is a realistic passenger vehicle model based on the geometries of two medium sized cars, the Audi A4 and the BMW 3 series, respectively. The DrivAer model comes in three configurations, the Fastback model, the notchback model, and the estate back model [2]. Figure 1-2 shows the fastback model.

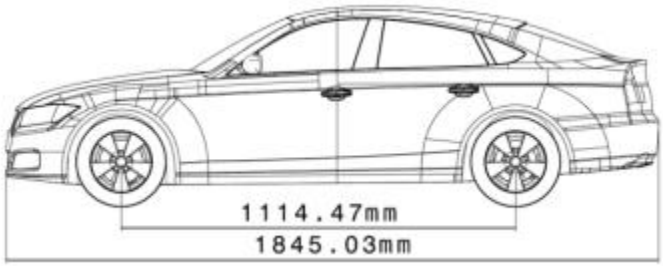

Figure 1-2: DriveAer Model [2]

Experimental studies conducted by Heft *et al*. [2] provide good data regarding the overall aerodynamic phenomenon around the vehicle body. This model also comes with the advantage of a plethora of independent research projects conducted using it. This makes available, a variety of good information that can be used to set up an adequate computational model.

1.2.2 Tire Features

Previous work conducted by Lee Axon *et al.* [3] have shown the differences in the flow structures around stationary and rotating tires investigating the jetting effect. Through CFD studies it was shown that the rotating tire would have a lower aerodynamic drag compared to a stationary one. Studies conducted by P Lenewicz *et al.* [4] have shown that the grooved tire would have lower drag compared to a slick tire. This was shown to be due to the jetting effect associated with a slick tire. Tunnel studies conducted by Christoffer Landstrom *et al.* [5,6,7] have shown variances in results due to rim designs. Considering the components of an isolated tire such as the lateral

grooves, the rim design and the contact patch of the tire seems important in order to attain reasonable results.

1.2.3 Computational Techniques for Vehicle Simulations

Studies by Ashton and Revell *et al.* [8,9] discuss the comparison of RANS and DES methods for computational simulation of the DrivAer body. The results from their study highlight the acceptability of the usage of RANS models for computational fluid dynamics analysis around vehicles. Ashton and Revell *et al.* [8,9] point to the shortcomings of the RANS models, which they state stems from the RANS models' inability to properly capture the flow separation regions around the vehicle. However, RANS methods work well for the fastback DrivAer model. Soares *et al.* [10,11], in their study, mention the relative simplicity of the flow around the fastback configuration of the DrivAer model due to its streamlined geometry. They further discuss the usage of a realizable k-epsilon model and its robustness over the k-omega model when cost of computational analysis is considered.

1.2.4 Computational Techniques for Standalone Tire Simulations

More recent studies conducted on the isolated tires have discussed different computational methods for solving flow around a tire. Jan Reiss *et al.* [12] and their group have used the Delayed Detached Eddy Simulations (DDES) as the turbulence model with the near wall regions solved using the Spalart-Allmaras RANS turbulence model. Eliminating the need to fully resolve the boundary layer. Heo *et al.* [13] used an RNG k-epsilon model for their simulation of flow around an isolated tire. The RNG k-epsilon model provides better results than the standard k-epsilon model for flow fields containing higher streamline curvature and separation. Schnepf *et al.* [14] has used a similar model for their studies. Zhou *et al.* [15] has shown that the SST k-omega model used with the Improved Delayed Detached Eddy Simulation model improves the separation prediction in the near wall region and provides a flexible and convenient scale resolving simulation model for airflow with a high Reynolds number. Adit Sunil Misar *et al.* [16] notes that the SST k-omega model is better suited for the simulations because it blends a k-epsilon model in the far field free stream while keeping the k-omega boundary layer calculation advantages in the near wall region.

1.2.5 Validation

Vehicle Assembly

Experimental studies were conducted by Heft *et al.* [2] on the DrivAer model in wind tunnel A at the Institute of Aerodynamics and Fluid Mechanics at TU Munich. The goal of their study was to present the DrivAer model to a broad audience and to discuss its development. The study presents experimental force and pressure measurement which includes coefficient of pressure and coefficient of drag data. This data is used in our study for the validation of our baseline computational model. This gives us a better understanding of the accuracy of our solution model derived from literature review.

Instrumentation and Measurement

Figure 1-3: Experimental Setup for Vehicle Body [2]

As shown in Figure 1-3, the DriveAer model in the wind tunnel is held from above with a central strut and each of the wheels is supported by four separate horizontal struts. A moving belt is placed below rotating tires to simulate the vehicle moving forward.

For force measurements, a main internal 6-component force balance is placed between the top strut and the model, and four separate 1-component force balances are attached to the wheels. The forces of all balances were added up and averaged over measurement intervals of 10s each.

For pressure measurements, a multiport pressure measurement system is used. The system is connected to surface pressure taps through flexible tubing. For the time averaged measurements, a sampling rate of 20 Hz and an average period of 10s were chosen.

Standalone Tire

For a quantitative validation of the standalone tire model, a study by schnepf *et al.* [25] was used. In this study, two special mounts were used in the AEROLAB wind tunnel for a standalone tire as shown in Figure 1-4. The tire is driven by a treadmill and has a vertical preload. This accurately simulates for deformation under load for a rotating tire.

Figure 1-4: Standalone Tire Experimental Setup [25]

The study used measurement probes for the standalone tire in order to calculate the flow features around the tire as shown in Figure 1-5. 12-hole probes were used due to their large measuring range in the downstream region. The measured data was then used to calculate forces. The coefficient of drag data from this study is used to validate the standalone tire model in this study.

Figure 1-5: Tire Experimental Setup with Probes [25]

For a more qualitative analysis, another study by Schnepf *et al.* [14] was used to compare the coefficient of pressure trend in the wake plane of the tire. The study uses computational methods to simulate for the flow around the tire using Exa PowerFLOW 5.0. The computational study was based on the Lattice – Boltzmann method. This method is derived from the statistical description of microscopic particle dynamics following the kinetic gas theory.

1.2.6 Parametric Model

A parametric study of the tire is conducted to understand and analyze the drag performance of the tire. Previous studies have considered the wheel shape factors, such as wheel opening area, wheel ring and ring width for parametric studies based on the wheel drag performance [17].

To conduct parametric studies on both the rim protector design as well as the overall tire design, two baseline geometric models are considered, a tire – vehicle geometry from the DrivAer model for the overall tire parametrization as well as a (225/55R17) tire model for the rim protector parametrization.

Parametrization of the Overall Tire

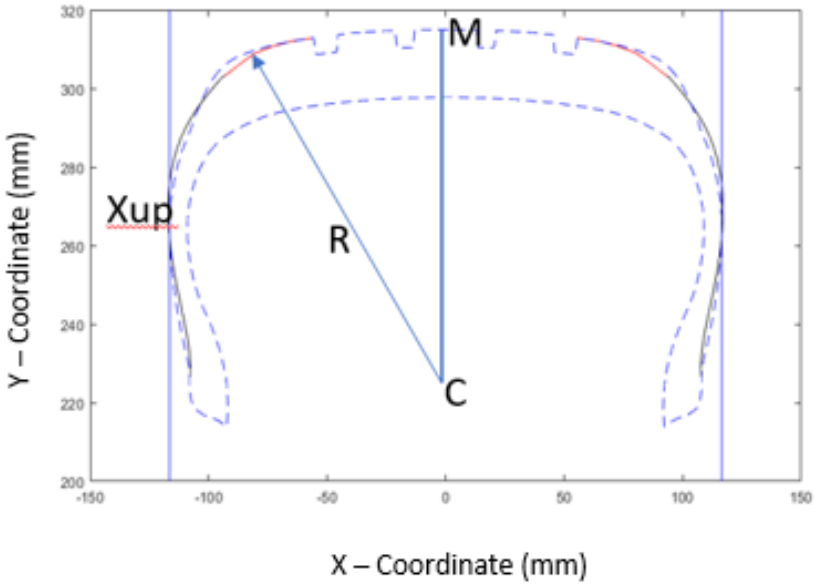

Figure 1-6: Tire Parameters

To conduct a parametric study, the three parameters selected are Xup, Shoulder Radius (R) and CM as shown in Figure 1.6. Here Xup is the x coordinate value of the sidewall outline as we go up in the y direction. The variables Xup and CM dictate the sidewall profile [18,19].

Parametrization of the Rim Protector

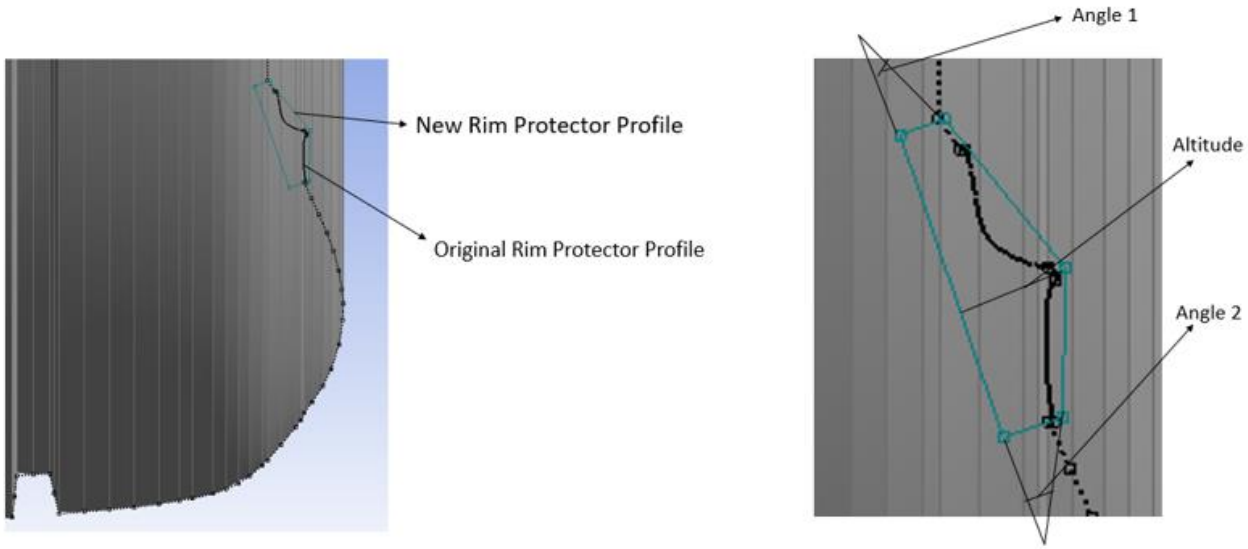

Figure 1-7:Rim Protector Cross Sectional Profile (Left), Rim Protector Parametrization (Right)

Rim protectors are an added piece of reinforced rubber around the contact area of the tire and the

wheel. This protrusion in the wheel cross section helps prevent curbing, creates a seal that protects against wheel corrosion, and reduces the severity of bulges and cracks due to uneven forces acting on the tire.

The rim protector cross sectional profile is quite complicated and hence its parameterization is also quite complicated. In order to resolve this issue, the rim protector cross sectional profile is simplified to pentagon, which can be extended to a triangle.

The shape of this extended triangle now dictates the shape of the rim protector cross sectional profile. To parametrize this profile, we use the base angles of the extended triangle and the altitude of this triangle as the parameters. Figure 1.7 shows the three parameters that will be used in the sensitivity study.

Chapter 2: Design and Models for the Tire – Vehicle Assembly

2.1 Design Model

2.1.1 Geometry

Considering the tradeoff between the computational cost, robustness of the model, and the accuracy of results, the Fastback configuration of the Driver model has been selected.

The features selected for the tire-vehicle assembly model are: (1) the mirrors, (2) a smooth underbody for easier meshing, and (3) no internal components, as they will not affect the flow around the body, since our solution does not use the energy equation.

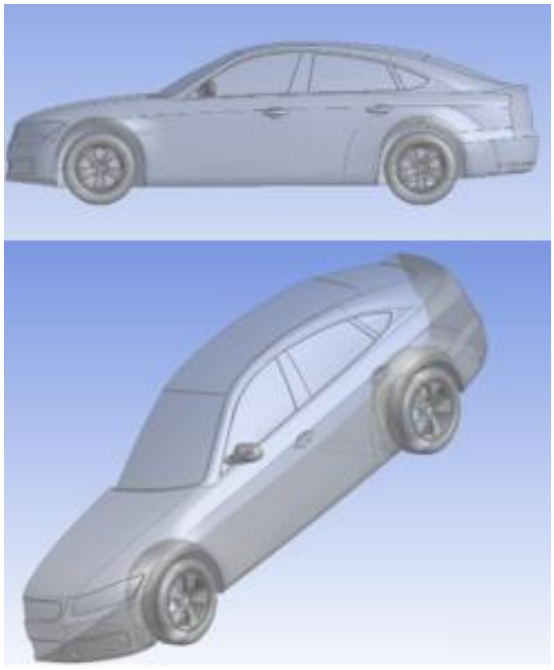

Figure 2-1: Geometry of the DrivAer Fastback model

The flow domain is chosen to represent the open road. In order to simulate the open road, a simplistic cuboidal enclosure is selected to bound the computational model. The dimensions of the enclosure were selected to guarantee that the flow is fully developed. The blockage ratio, given by the ratio of the frontal projected area of the vehicle to the frontal projection area of the flow domain, is another factor that decided the overall dimensions of the enclosure in order to best mimic open road conditions [20,21,22].

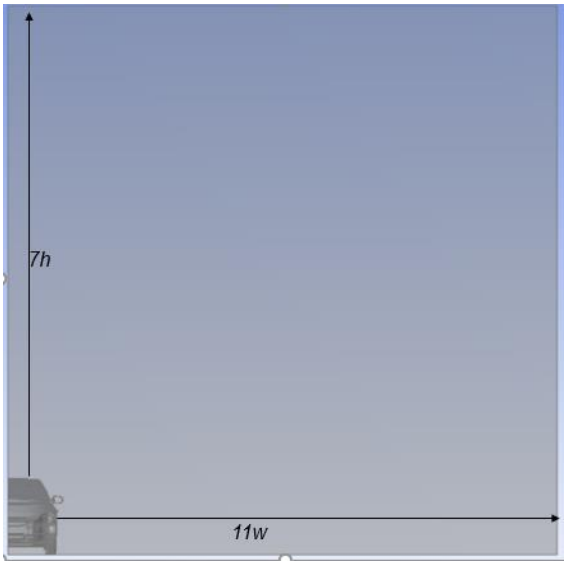

Figure 2-2: Frontal Dimensions of the Cuboidal Enclosure

As calculated, the blockage ratio is approx. 0.00543. In Fig.3, parameter w represents the width of the entire vehicle, while h is the height of the vehicle. As can be seen in Figure 2.2, the flow domain was extended 10 car lengths behind the fastback DriveAer model and had 4 car lengths for the flow entrance length.

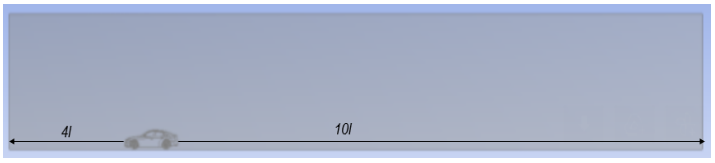

Figure 2-3: Side Dimensions of the Cuboidal Enclosure

2.1.2 The Contact Patch

The contact patch modelling is one of the most important facets of the tire-vehicle geometry since it dictates the interaction between the moving ground and the rotating tires. A plethora of studies have been conducted in order to fine tune and most accurately model the tire contact patch [22]. As shown in Figure 2-4, a flat geometrical extension of the tire model was used since our focus is the drag performance of the vehicle. Having a simplified and static contact patch would ease the

computational burden, as well as the meshing process.

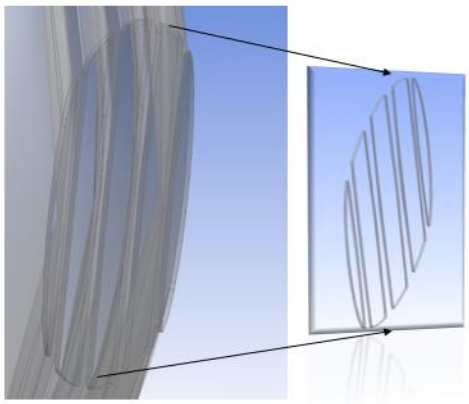

Figure 2-4: Tire-Ground Contact Patch Mode

2.2 Mesh Design

2.2.1 The Mesh Development

The mesh parameters for the model are based on the study conducted by Soares *et al.* [10,11] with minor modifications made in order to reach convergence. Figures 2.5 and 2.6 showcase the mesh created for one of the final cases in the parametric study.

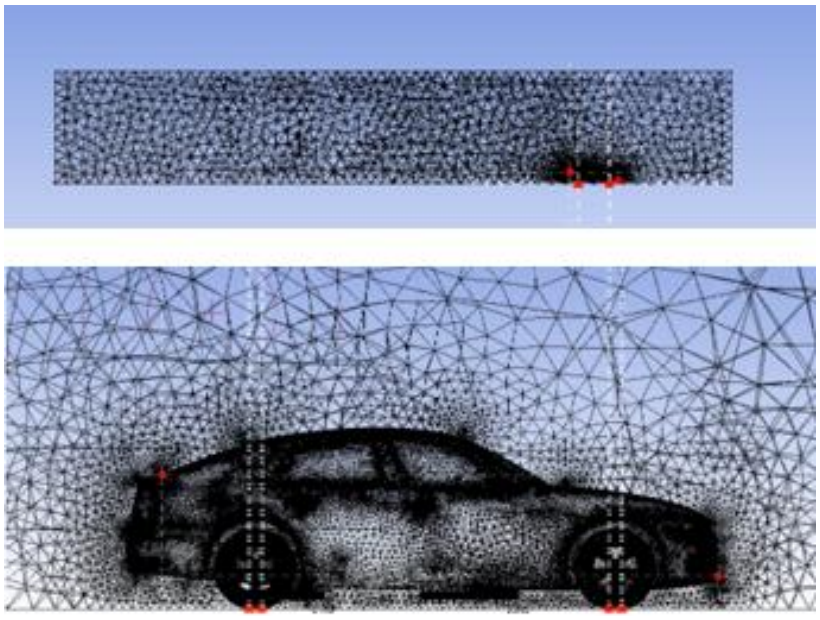

Figure 2-5: Grid Used for Simulations

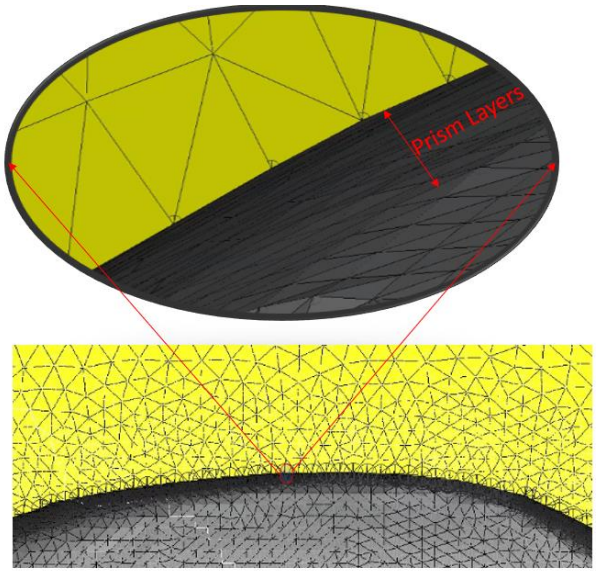

Figure 2-6: Inflation Layers

Tables 2.1 and 2.2 show the mesh parameters used in order to simulate the tire-vehicle assembly. Tetrahedral elements were used to discretize the flow domain. Inflation layers with a first prism layer thickness of 0.5 mm for 15 layers were used to better capture the details of the boundary layers. The final mesh turned out to have 42 million grid elements based on the resulting inflation layers and the face sizing of the various facets of the assembly geometry.

Table 2-1: Mesh Sizing for Named Selections of the Geometry

Mesh Parameters for Named Selections (Sizing)	
Car Body Face Sizing	0.01 mm
Tire Face Sizing	0.001 mm
Contact Patch Face Sizing	0.0001 mm
Mirror Face Sizing	0.001 mm
Enclosure Face Sizing	0.1 mm

Table 2-2: Mesh Parameters for the Vehicle Model

Mesh Parameters	
First Prism Layer Thickness	0.5 mm
Number of Prism Layers	15
Number of Mesh Elements	42 million
Growth Rate	1.72

2.2.2 Mesh Convergence

Coefficient of drag data is used to verify our results. Table 2.3 shows the drag coefficient values for different mesh levels.

Table 2-3: Grid Convergence Results

Mesh Level (Number of Mesh Elements)	Drag Coefficient
0.7 million	0.310
2.1 million	0.302
3.5 million	0.290
17 million	0.252
21 million	0.245
42 million	0.244

It can be seen that we approach convergence at 42 million mesh elements. The simulation was done for the moving ground rotating wheel boundary conditions and a transient time regime with a time step of 10^{-4}s. We use the realizable k-epsilon model for our simulations.

2.3 Numerical Methods

2.3.1 The Governing Equations

Based on the freestream conditions, we use an incompressible flow model [10,11]. The Navier Stokes equations reduce to

$$\frac{\partial u_i}{\partial x_i} = 0 \tag{1}$$

$$\frac{\partial u_i}{\partial t} + \frac{\partial}{\partial x}\left(u_i u_j\right) = -\frac{\partial P}{\partial x_i} + \frac{\mu}{\rho}\frac{\partial^2 u_i}{\partial x_i \partial x_j} \tag{2}$$

We use the following formulation for the coefficient of drag.

$$C_D = \frac{F_D}{\frac{1}{2}\rho_\infty A_{proj} {U_\infty}^2} \tag{3}$$

where F_D is the drag force, and U_∞ represents the freestream velocity of air.

To calculate the drag area A_{Drag}, the following equation is used.

$$A_{Drag} = A_{proj} C_D \tag{4}$$

where C_D is the coefficient of drag.

Here, A_{Drag} is the drag area defined by the projected area multiplied by the coefficient of drag. A_{proj} is the projected frontal area. U is the x direction velocity in a cartesian system and ρ is the density of the fluid that is air. The material used for the car body is aluminum.

2.3.2 Simulation Models and Methods

Table 2.4 lists the parameters used for the unsteady RANS based transient simulations. Soares *et al.* [10,11] has shown that the K-epsilon model is more robust for simulating the fastback assembly model compared to the k-omega model considering the cost of computation.

Table 2-4: Solution Model for Simulation

Model	Conditions
Domain	Open Road
Time Regime	Transient, time step: 10^{-4}s
Flow Regime	Turbulent
Turbulence model	Realizable K-epsilon model

2.3.3 Boundary Conditions

Table 2.5 shows the boundary conditions setup. The vehicle velocity which corresponds to the moving ground translational velocity as well as the tire rotational velocity are 44.2 m/s and 347.5 rad/s, respectively for validation simulations. An inlet velocity of 44.2 m/s is used for the validation study whereas an inlet velocity of 36 m/s is used for the final parametric study.

Table 2-5: Boundary Conditions

Walls/Boundary	Conditions
Car Body	No slip
Tire	Rotational, no slip, 347.5 rad/s
Contact Patch	Static, no slip
Ground	Translating, no slip, 44.2 m/s
Inlet	Velocity, 36 m/s
Outlet	Pressure
Side and Top Walls	Symmetry

2.3.4 Parametric Study

To conduct a parametric study, the three parameters selected are Xup, Shoulder Radius (R) and CM as shown in Figure 2.7. Here Xup is the x coordinate value of the sidewall outline as we go up in the y direction. The variables Xup and CM dictate the sidewall profile. [18,19]

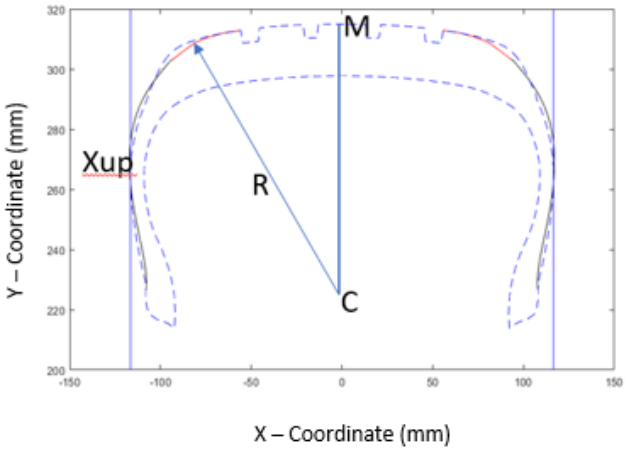

Figure 2-7: Tire Parameters

A Design of Experiments parametric model was set up using the Design Explorer module in ANSYS. Table 2-6 shows the range of the three parameters chosen for this study. The ranges of the three parameters are chosen to maintain geometric viability. ANSYS uses this information, as well as the generated drag area results to conduct a sensitivity analysis using the response surface function.

Table 2-6: Parameter Ranges

Parameter	Range
Shoulder Radius	190 mm to 210 mm
CM	190 mm to 200 mm
Xup	0.3 to 0.6

Chapter 3: Design and Models for the Standalone Tire

3.1 Design Model

To accurately represent the tire for reasonable results, we include symmetrical grooves along the tire, a shaft attached to the tire similar to a tire – vehicle geometry, a contact patch as well as a cuboidal geometry for an enclosure in order to simulate for open road conditions. The tire model used is (225/55R17).

Figure 3.1 represents the tire geometry which includes the previously mentioned geometrical features.

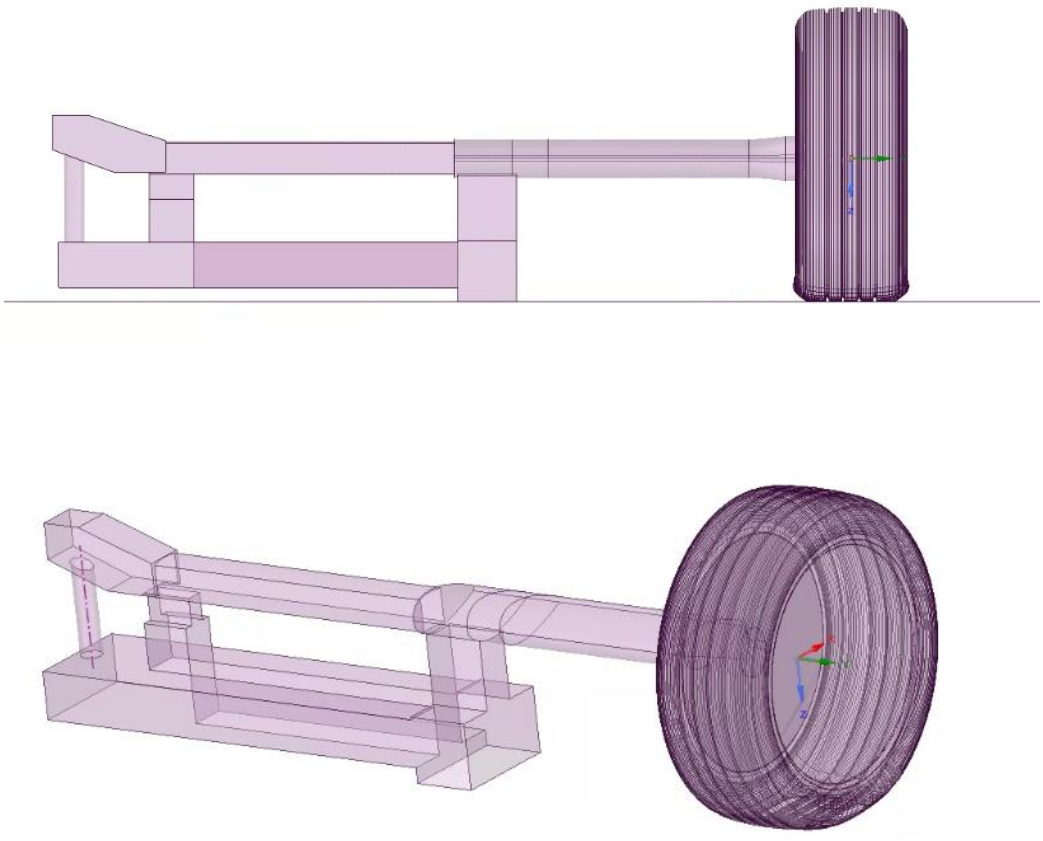

Figure 3-1:Standalone Tire

From Figure 3.2, it can be seen that the near contact patch region of the tire is modelled as if it had

a bulge on either side to accurately depict the deformation of the tire near the tire-road contact. Figure 3.3 shows the contact patch geometry of the tire. The contact patch is modelled as a small step at the bottom of the tire which is stationary while the rest of the tire rotates.

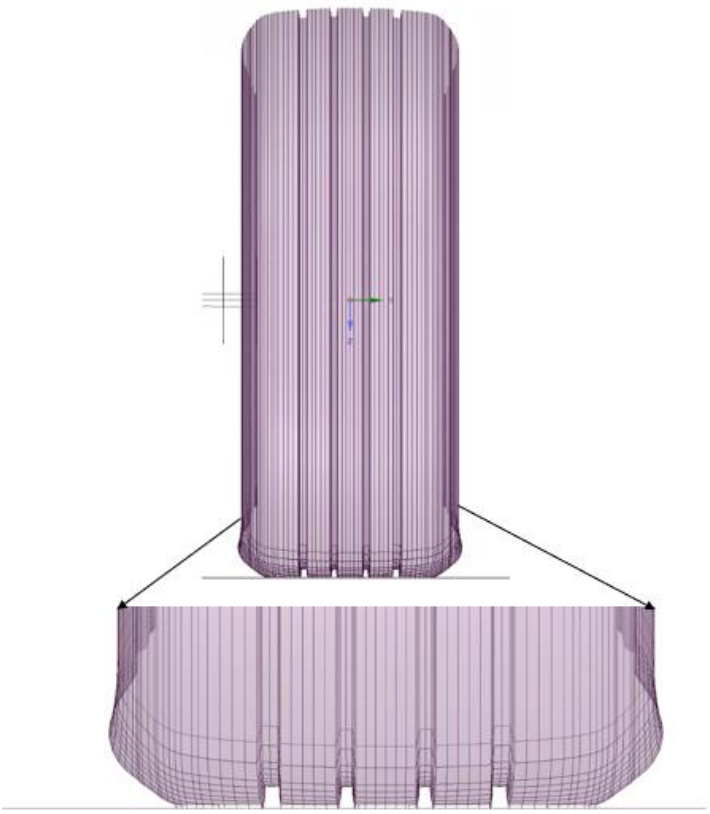

Figure 3-2: Geometry near tire-road contact

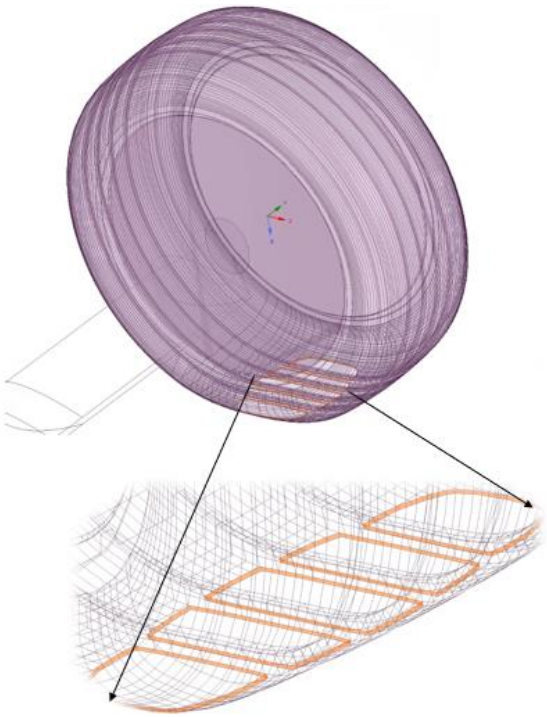

Figure 3-3: Contact Patch

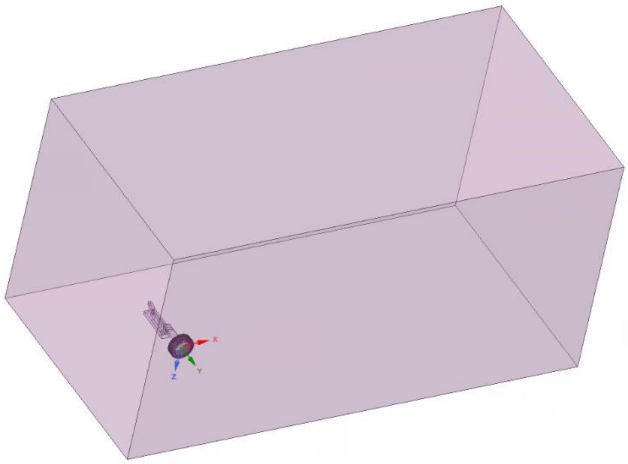

Figure 3-4: Tire in the flow domain

In Figure 3.4, the enclosure that the tire is simulated within is shown. This enclosure is the region of fluid, in this case air, flow. Since it is computationally expensive to include the geometrical features within a wind tunnel, this simplistic cuboidal enclosure is used as the flow domain. The dimensions of the enclosure were selected to ensure that the flow is fully developed. The blockage

ratio, given by the ratio of the frontal area of the tire model and the frontal area of the enclosure is considered. In this case, the projected frontal area of the enclosure is much larger than the projected frontal area of the tire [20,21,22]. Hence, it is a good representation of open road conditions.

3.2 Governing Equations and Boundary Conditions

3.2.1 Governing equations

In order to conduct a transient simulation, the governing equations solved were:

$$\frac{\partial \rho}{\partial t} + \frac{\partial \rho u_j}{\partial x_j} = 0 \tag{5}$$

$$\frac{\partial \rho u_i}{\partial t} + \frac{\partial}{\partial x_j}\left(\rho u_i u_j\right) = -\frac{\partial P}{\partial x_i} + \frac{\partial \left(T_{ij}\right)}{\partial x_j} + b_M \tag{6}$$

Here, u is the velocity vector, ρ is the density, b_M is the external force and T is the stress tensor given by:

$$\boldsymbol{T} = \mu\left(\boldsymbol{\nabla U} + (\boldsymbol{\nabla U})^T - \frac{\mathbf{2}}{\mathbf{3}}\boldsymbol{\delta}\,\boldsymbol{\nabla}\,.\,\boldsymbol{U}\right) \tag{7}$$

$$A_{Drag} = A_{proj} C_D \tag{8}$$

Here, A_{Drag} is the drag area defined by the projected area multiplied by the coefficient of drag. A_{proj} is the projected frontal area.

3.2.2 Boundary Conditions for Simulations

Table 3.1 shows the boundary conditions used for the simulation of the isolated tire model. These boundary conditions are based on a rotating tire, moving ground and a large flow domain.

Table 3-1: Boundary Conditions

Walls/Boundary	Conditions
Tire	Rotational, no slip, 144 rad/s
Contact Patch	Static, no slip
Ground	Translating, no slip, 36 m/s
Inlet	Velocity, 36 m/s
Outlet	Pressure

3.2.3 Parametric Study

In this study, the goal is to parametrize and conduct a sensitivity study on the rim protector design. From Figure 3.5, we can see that the rim protector cross sectional profile is quite complicated and hence its parameterization is also quite complicated. In order to resolve this issue, the rim protector cross sectional profile is simplified to pentagon, which can be extended to a triangle.

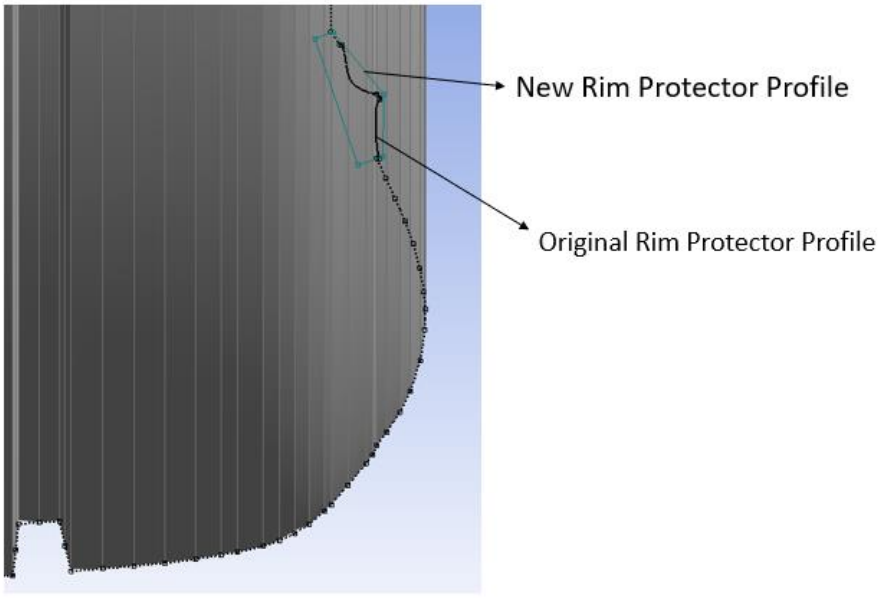

Figure 3-5: Rim Protector Cross Sectional Profile

The shape of this extended triangle now dictates the shape of the rim protector cross sectional

profile. To parametrize this profile, we use the base angles of the extended triangle and the altitude of this triangle as the parameters. Figure 3.6 shows the three parameters that will be used in the sensitivity study.

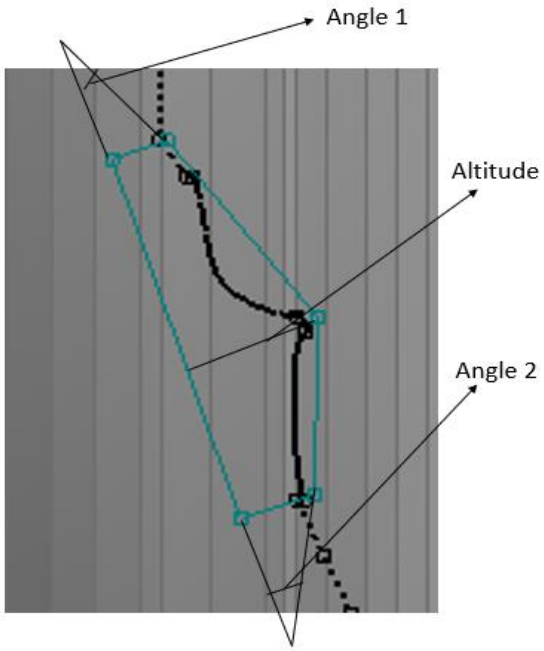

Figure 3-6: Rim Protector Parametrization

Design Of Experiments

With these parameters, a Design of Experiments model was set up. To create a design space, we use the Kennard-Stone Algorithm [23,24] for a 5^3 model. This method uses the distance in the design space consisting of 10 points with 3 degrees of freedom to select only the points which have the most distance between each other. The algorithm which was used to map out the design space concluded that in order to have 10 increments for the angle parameter and 6 increments for the altitude parameter, 15 simulations were sufficient for adequately representing the effects of parameter change.

Kennard-Stone Algorithm Implementation

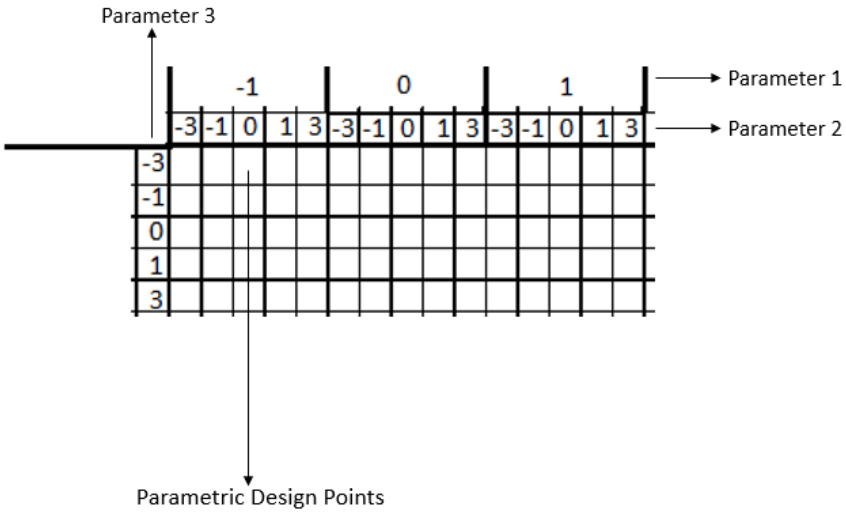

Figure 3-7: 3D Matrix for Kennard-Stone Algorithm [23,24]

Since there are 3 parameters and N distinct points based on the parametric range and the parameter increments, as shown in Figure 3-7, a 3-dimensional matrix is created. The matrix shown in Figure 3-7 is an example matrix for the purpose of understanding the procedure. The n < N design points for the design space are then chosen sequentially.

For each design point choice, points are selected with the aim of having the design points uniformly spaced over the matrix. To do this, the first two candidate points are chosen that are the farthest and each consequent point is chosen, keeping in mind that those remaining points have to be the farthest from an existing design point.

Parametric Range Calculation

The ranges of the parameters for the rim protector are calculated on the basis of two cases, the minimum viable rim protector protrusion case and the maximum viable rim protector protrusion case. The minimum protrusion case is based on the minimum effective protrusion of the rim protector that has a significant impact on the tire drag output. The maximum protrusion of the rim protector is when the rim protector bulges out to the end of the tire cross section.

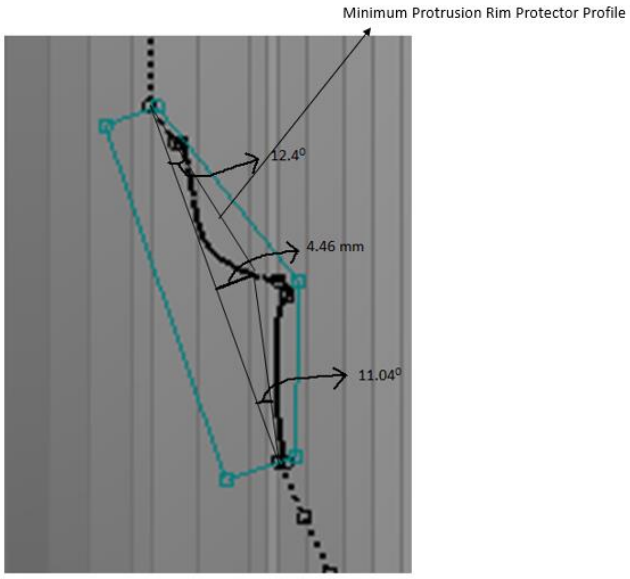

Figure 3-8: Minimum protrusion Rim-Protector Profile

Figure 3.8 shows the minimum protrusion case. Through transient simulations, the coefficient of drag for the tire without a rim protector was found through simulations. This was then compared to minimal increases in the three parameters for the rim protector. It was seen that only when angle 1 was increased to 12.4^0, angle 2 to 11.04^0 and altitude to 4.46 mm, there was a percentage difference of >2%. These values were then chosen to be the parameter values for the minimum protrusion case.

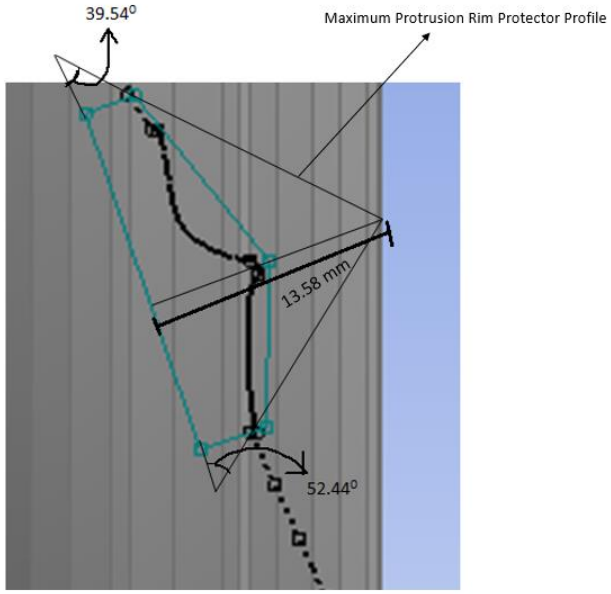

Figure 3-9: Maximum protrusion Rim-Protector Profile

Figure 3-9 shows the maximum protrusion case of the rim protector when the rim protector cross sectional profile bulges out to the edge of the tire cross section.

Based on these two cases, Table 3.2 shows the range of the three parameters included in this design of experiments sensitivity study.

Table 3-2: Parameter Ranges

Parameter	Range
360 - Angle 1	320.46^0 to 347.60^0
360 - Angle 1	307.56^0 to 348.93^0
Altitude	4.46mm to 13.58mm

Chapter 4: Results and Discussion

4.1 Tire – Vehicle Assembly

In this section, the validation of the computational model is discussed. Results from the parametric study and a discussion of those results follow. For the validation of our model, we use experimental measurements of pressure and drag. The analysis is done based on the relative error percentage based on the experimental values, as well as comparison of the general trends of the flow features around the tire vehicle assembly.

For our results from the parametric study, we look at the calculated drag area values from our computational simulations. These values give us a better idea of the aerodynamic performance of the tire based on the parameter values.

4.1.1 Validation of Baseline Model

The validation study was conducted for the baseline case and was used to compare the numerical results generated with the experimental data reported by Heft *et al.* [2].

4.1.2 Coefficient of Drag Calculations

Experimental results [2] show that the coefficient of drag result for the moving ground, rotating wheels' case is 0.243. From our computational simulations, we find that the coefficient of drag value for the vehicle is 0.244. Calculating the error percentage:

$$Error\% = \frac{|Experimental\ Result - Simulation\ Result|}{Experimental\ Result} * 100$$
$$= \frac{|0.243 - 0.244|}{0.243} * 100 = 0.41 \quad (9)$$

With an error percentage of 0.4%, the simulation methods are adequate for solving the flow around the tire-vehicle assembly. This is considering that we did not simulate a geometry that included features of a wind tunnel.

4.1.3 Flow Features around the Vehicle Body

Based on a study conducted by Soares *et al*. [10,11], one of the key assumptions was the accuracy of the realizable k-epsilon method for the simulation of the tire-vehicle assembly. The primary reason for using a realizable k-epsilon method is its low computational cost. However, if there is flow separation on the assembly, a hybrid RANS-LES method would be required. From Figure 4.1, we can see that there is little to no flow separation on top of the vehicle body. This helps us ascertain that a RANS realizable k-epsilon method is adequate for our simulations.

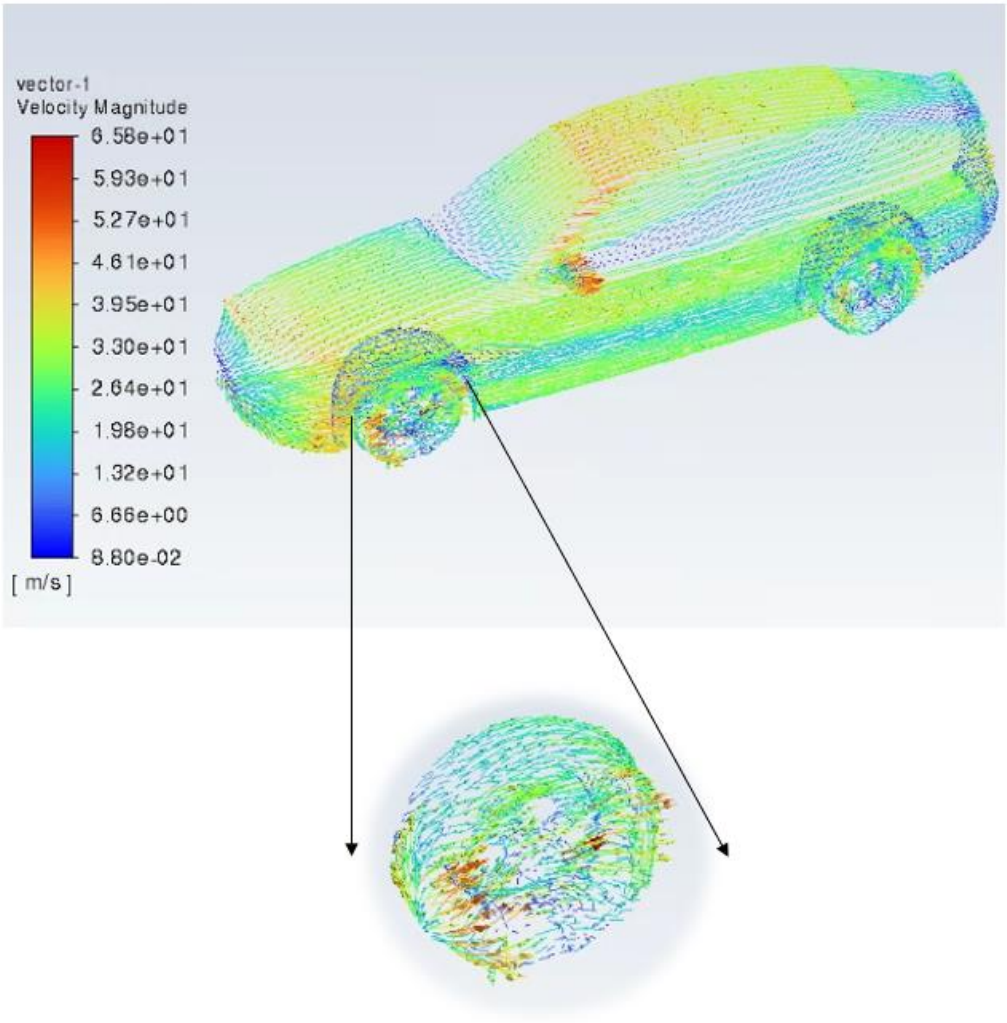

Figure 4-1: Velocity Streamline along the Vehicle with a zoomed in figure of the tire velocity magnitude contour.

Figure 4.2 shows a plot of the coefficient of pressure at the y=0 plane for the fastback configuration calculated using our computational simulations, as well as the experimental values calculated by Heft *et al.* [2]. The trend in the coefficient of pressure along the vehicle body from the Simulations are very similar to the experimental results. There are, however, some inconsistencies especially at the back of the vehicle. These inconsistencies can be attributed to the flow separation at the back of the vehicle, which is not captured by the RANS model. These inconsistencies are still very minute and are to be expected when comparing computational data to experimental data.

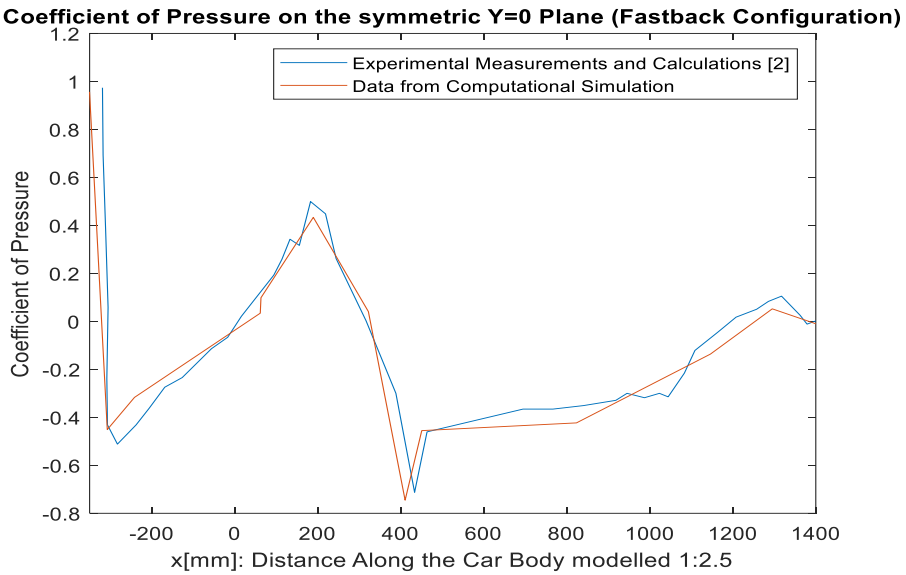

Figure 4-2: Coefficient of Pressure Distribution on y=0 axis along the car body

Figure 4.3 shows a pressure contour plot (Pa) for the vehicle body. This helps better understand the pressure distribution along the vehicle to get a general idea of the flow around the vehicle geometry and compare it with the general trend from the experimental data plotted in Figure 4.2.

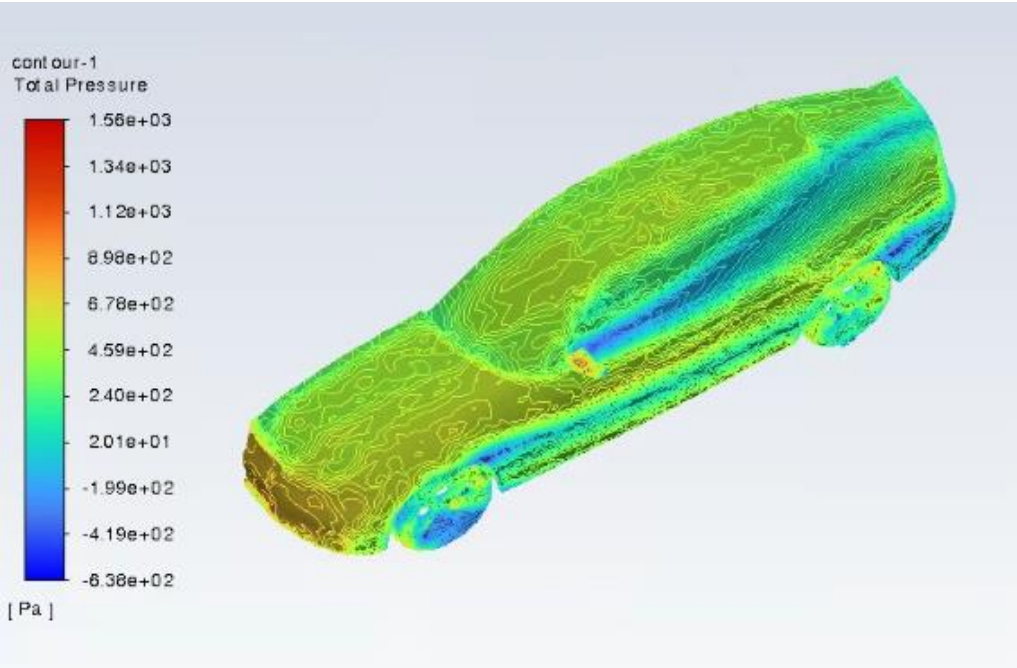

Figure 4-3: Pressure Distribution Contour along the Car Body

As observed, the static pressure value is largest at the front of the vehicle and the mirrors, but it decreases as we go to the middle of the car body. The pressure value then increases as we go towards the back of the vehicle. This is consistent with the data from Figure 4.2.

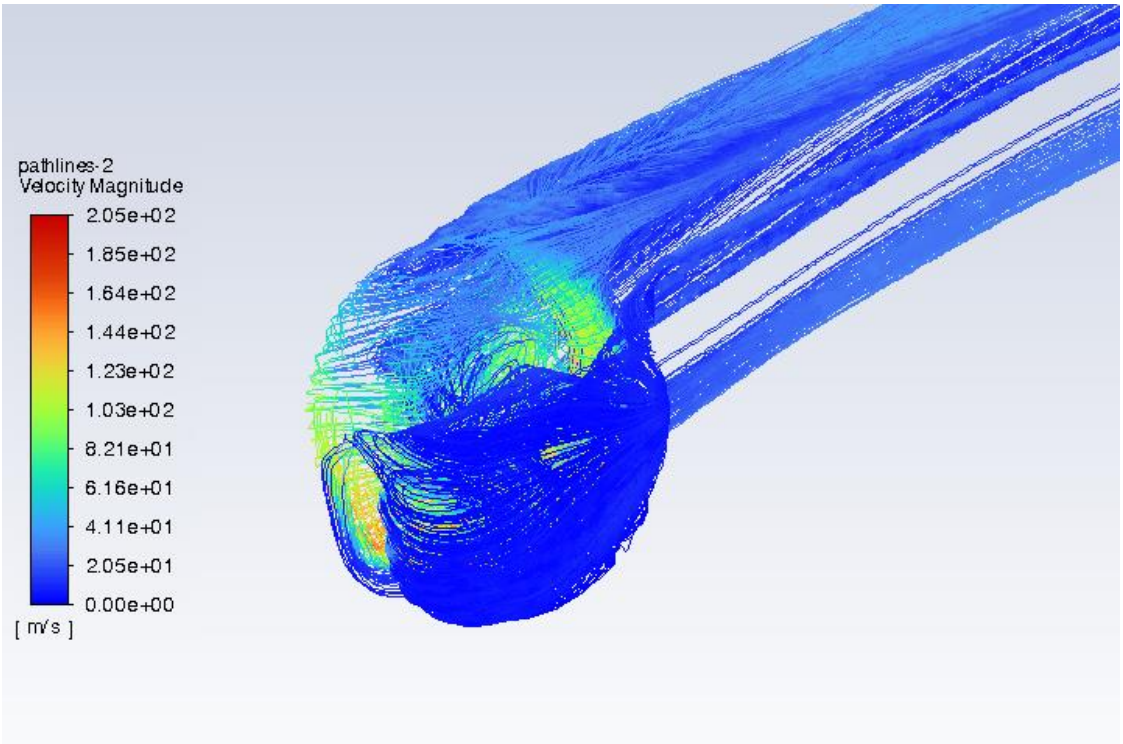

Figure 4-4: Velocity Streamlines of air along the front left tire of the vehicle

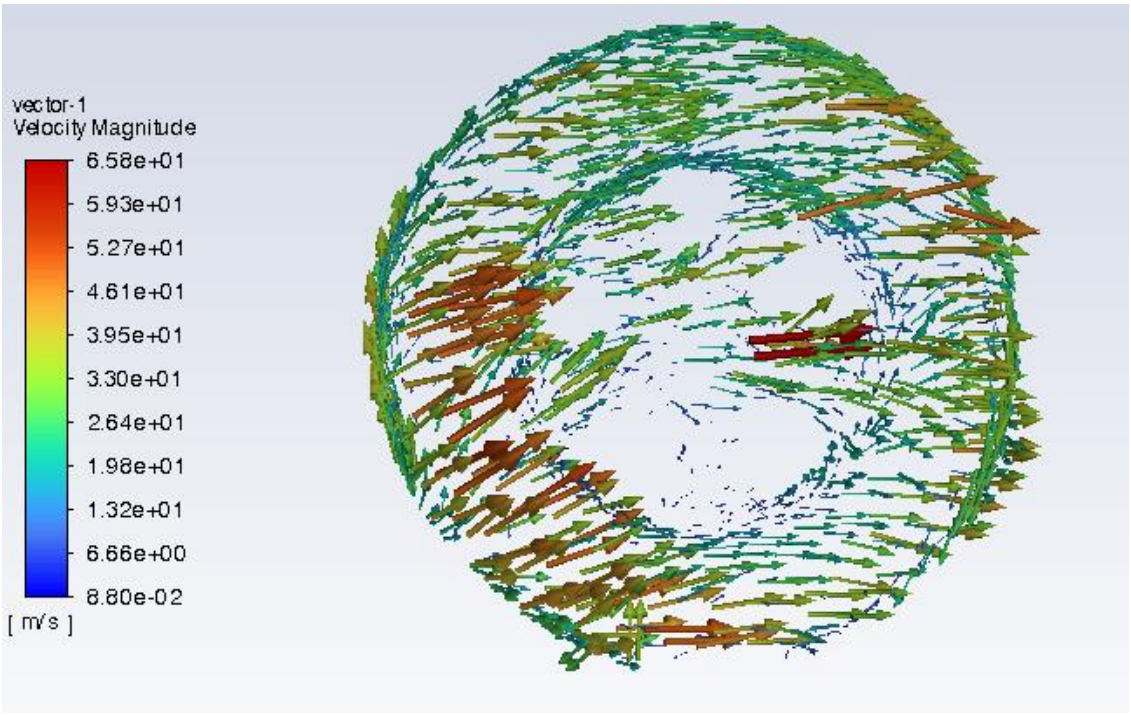

Figure 4-5: Velocity vectors of air along the front left tire of the vehicle.

The Figures 4.4 and 4.5 show the velocity streamlines as well as the velocity vectors around the tire. The velocity streamlines showcase the wake development and how it is affected by the car body interfering with the flow field. The velocity vectors give us a better idea of how the flow develops around the tire.

4.1.4 Results from the Parametric Study

The drag area was used to ascertain the drag performance of the vehicle. A design space was set up using ANSYS design explorer. To conduct a parametric study, the three parameters selected were Xup, Shoulder Radius (R) and CM. Here Xup is the x coordinate value of the sidewall outline as we go up in the y direction. The variables Xup and CM dictate the sidewall profile. [18,19]

Design of Experiments Regression Model

In order to conduct a detailed parametric study, the central composite design algorithm was used on Ansys Design Explorer. The central composite design algorithm is used to build a second order model for the output parameter in order to further conduct linear regression to obtain response surfaces. Upon using the central composite design algorithm, some of the design points were not geometrically viable for assembly with the vehicle. Hence, those design points were replaced with new design points based on a 3-D matrix of the design points using the Kennard-Stone algorithm. Hence, a third order regression analysis is used for this parametric study.

The third order model can be written in the equation form as follows,

$$Drag\ Area = Xup * A + CM * B + R * C + Xup^2 * D + CM^2 * E + R^2 * F + Xup^3 * G + CM^3 * H + R^3 * I + Intercept \quad (10)$$

As shown in equation 10, there is a cubic relationship between the parameters CM, Xup and R and the drag area. Here, A, B, C, D, E, F, G, H and I are coefficients to be determined through this regression analysis.

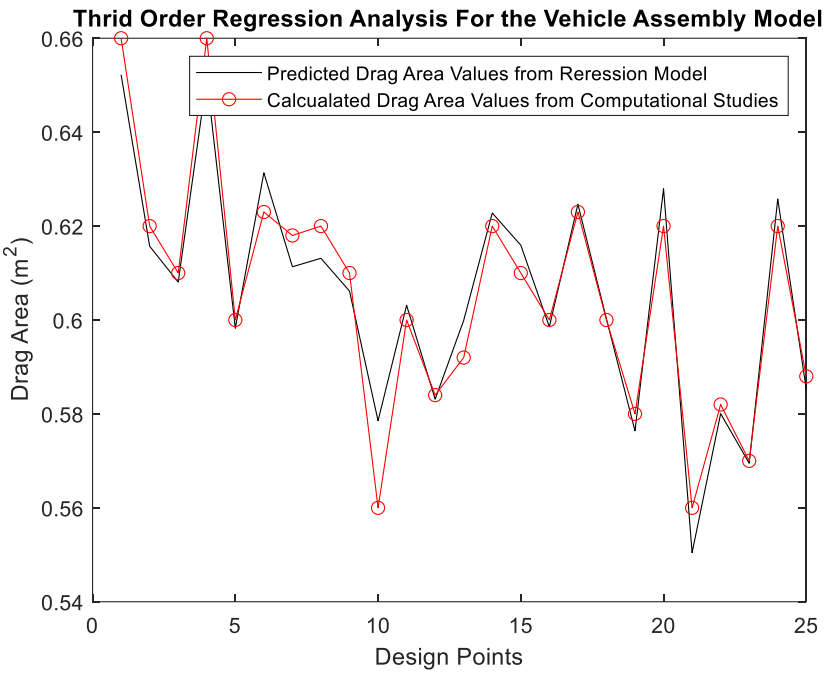

Figure 4-6: Comparison of Calculated Drag Area and Regression Predicted Drag Area

Upon conducting a regression analysis with the input and output data, it is seen that the regression model is able to successfully predict the drag area output with an R^2 value of 0.934 (Figure 4-6). The p value from this regression analysis is 0.00042 which is sufficient for this study.

Table 4-1: Equation Coefficients from Regression Analysis

	Coefficients
Intercept	-240.9182993
R	-0.362823693
CM	-0.497495406
Xup	4.035097045
R^2	0.001571312
CM^2	0.050039867
Xup^2	-0.020125552
R^3	-2.22754E-06
CM^3	0.436399854

Xup^3	3.34005E-05

Table 4-1 shows the coefficients as well as the intercept for the second order regression model.

Response Surfaces

The drag area results were used to check the impact rank of the parameters. Figures 4-7, 4-8 and 4-9 show the drag area results for the assembly model.

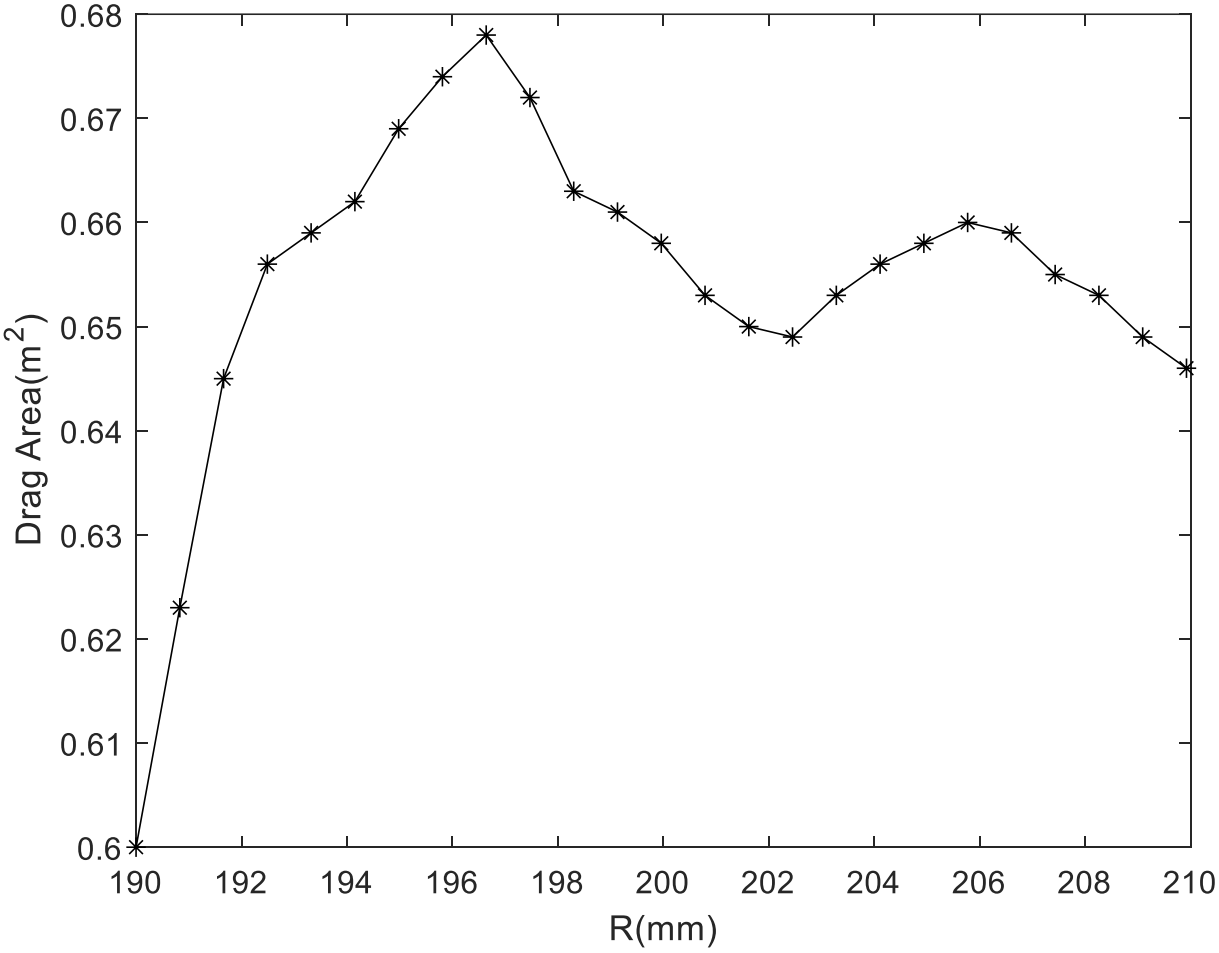

Figure 4-7: Drag Area values with changing Shoulder Radius.

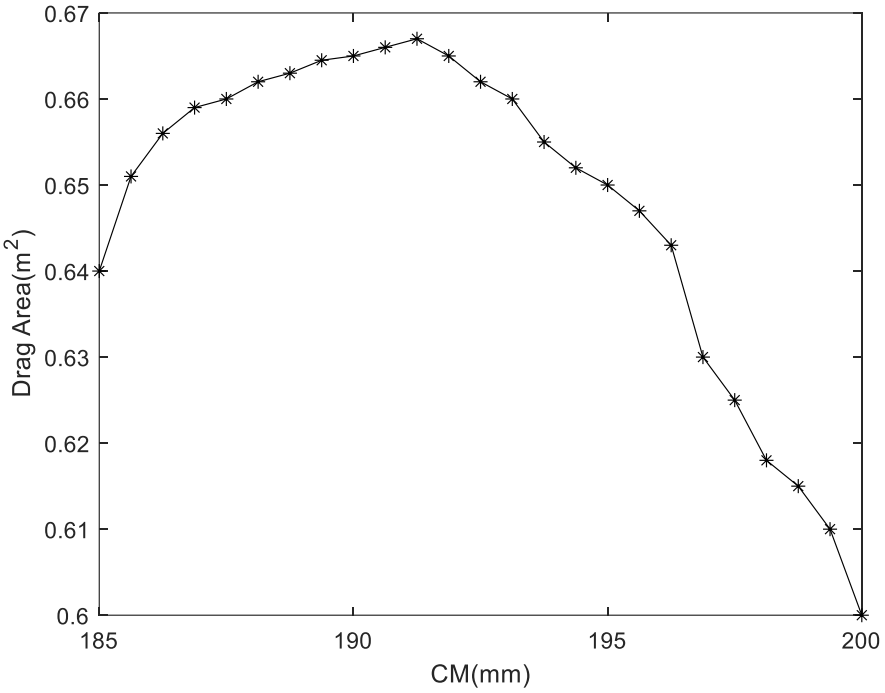

Figure 4-8: Drag Area Values with changing CM

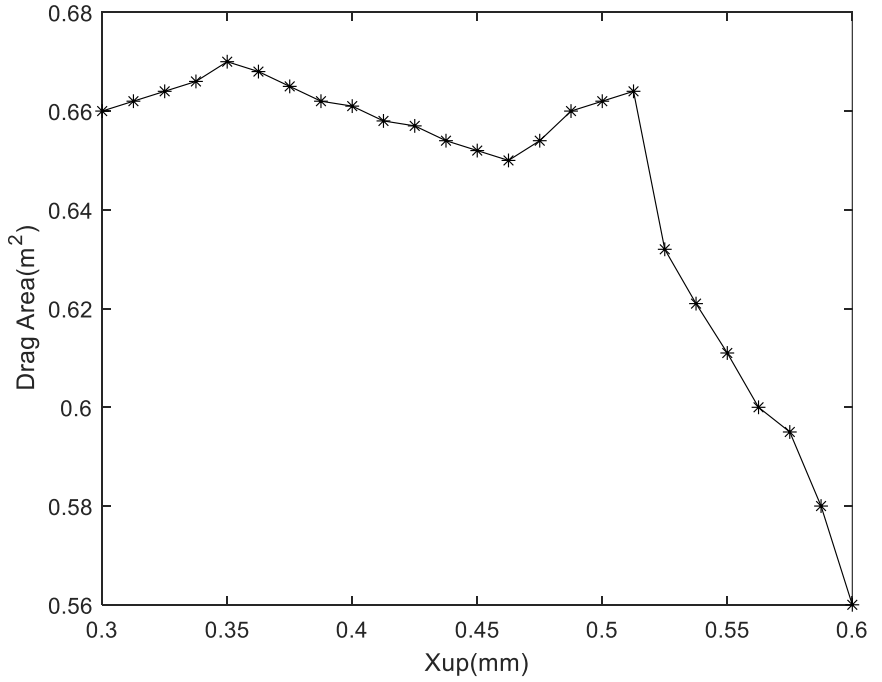

Figure 4-9: Drag Area Values with changing Xup

Figures, 4.6, 4.7 and 4.8, show the drag area variance as we vary the shoulder radius and the side wall profile (CM and Xup) of the tire, while keeping all the other parameters constant at baseline values. Results from 25 runs are used for these plots. From these figures, we can see those independent effects of the three parameters on the overall drag area of the assembly model. From these plots, we can observe that changing the shoulder radius and Xup within their respective ranges achieves the largest difference in drag area while changing the CM has a relatively smaller impact.

Figures 4.11, 4.12 and 4.13 are response surfaces based on the Design of Experiments conducted. The Method of Response Surfaces was used on ANSYS Design Explorer. The design space consisted of 25 design points. The drag area calculated was our output parameter with CM, Xup and R being the input parameters. Figure 4.10 shows the goodness of fit for the linear regression model used to build the response surfaces.

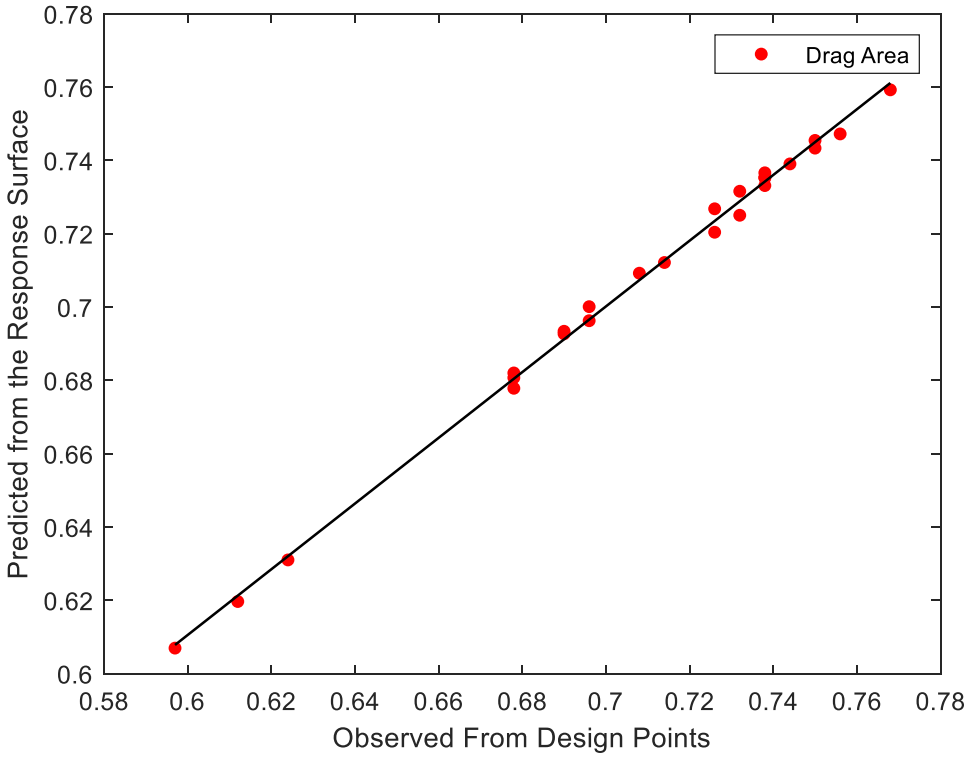

Figure 4-10: Goodness of Fit Plot for Drag Area Predicted from the Response Surfaces vs Drag Area Observed from the Design Points.

From the goodness of fit analysis, the Coefficient of Determination or the R^2 value found was 0.98. This shows that the response surface method is adequate for the representation of the impact of the three parameters that are being studied.

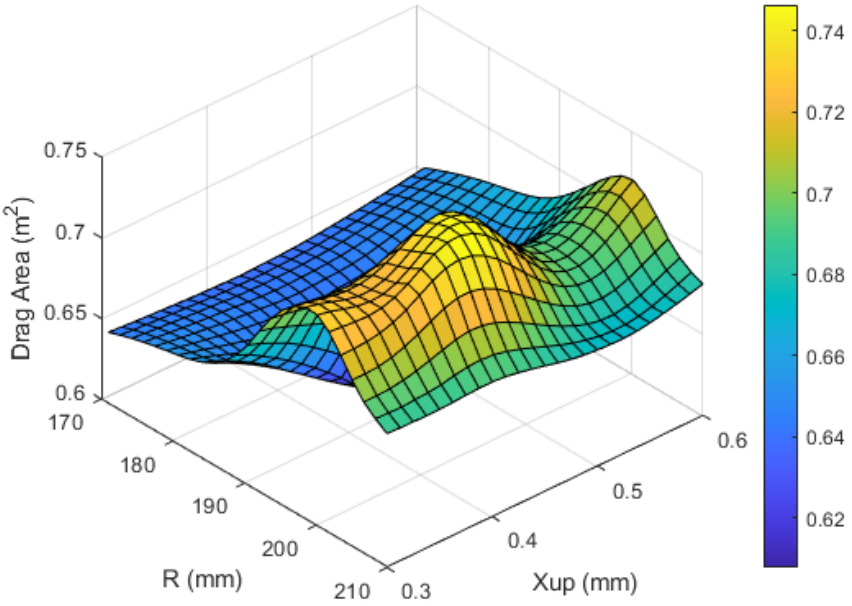

Figure 4-11: Response Surface Capturing the effect of Xup and R on the Drag Area

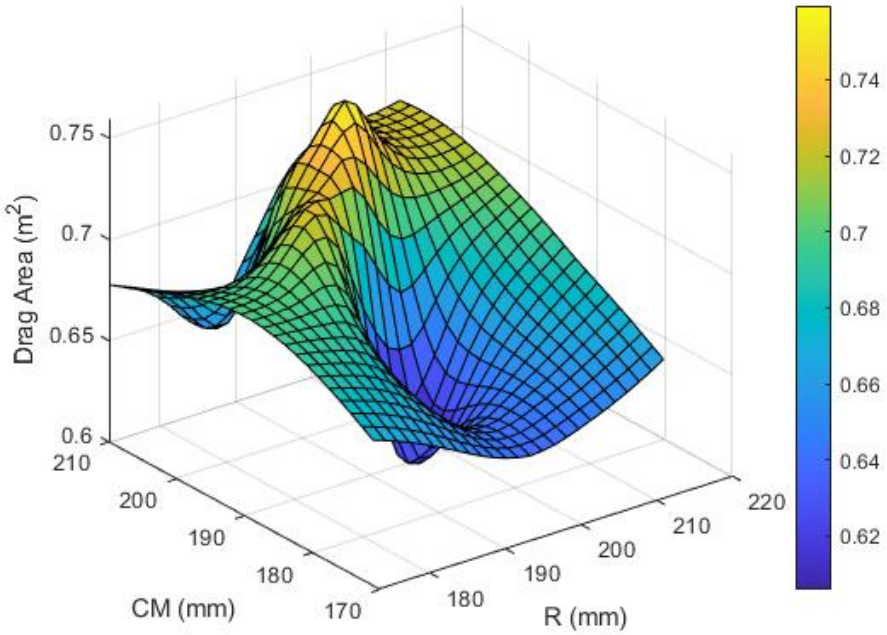

Figure 4-12: Response Surface Capturing the effect of CM and R on the Drag Area

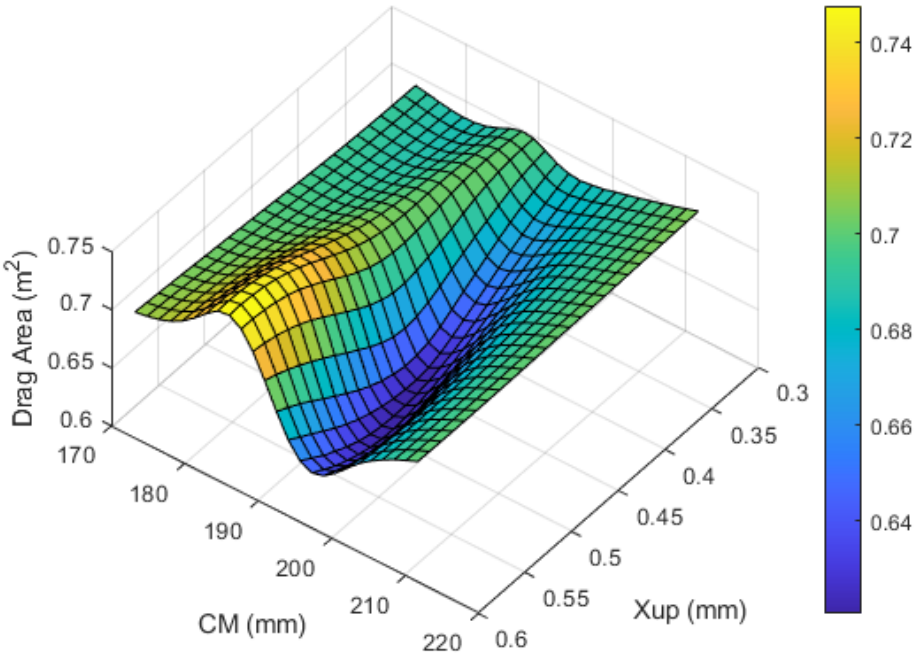

Figure 4-13: Response Surface Capturing the effect of Xup and CM on the Drag Area

These 3-D response surfaces each demonstrate the effect of changing the three parameters in pairs. From Figure 4.11, we can see that the drag area change due to the change in R is comparable yet larger than the change in drag area due to Xup. Whereas in figure 4.13, it is observed that the change in CM does not affect the change in drag area as much as the change in Xup. These plots give us a better insight into the impact of the three parameters on the drag area.

To better understand the sensitivity of these parameters a Design of Experiments needs to be conducted. Using a design space built by ANSYS Design Explorer, simulations for various combinations of the three parameters are conducted.

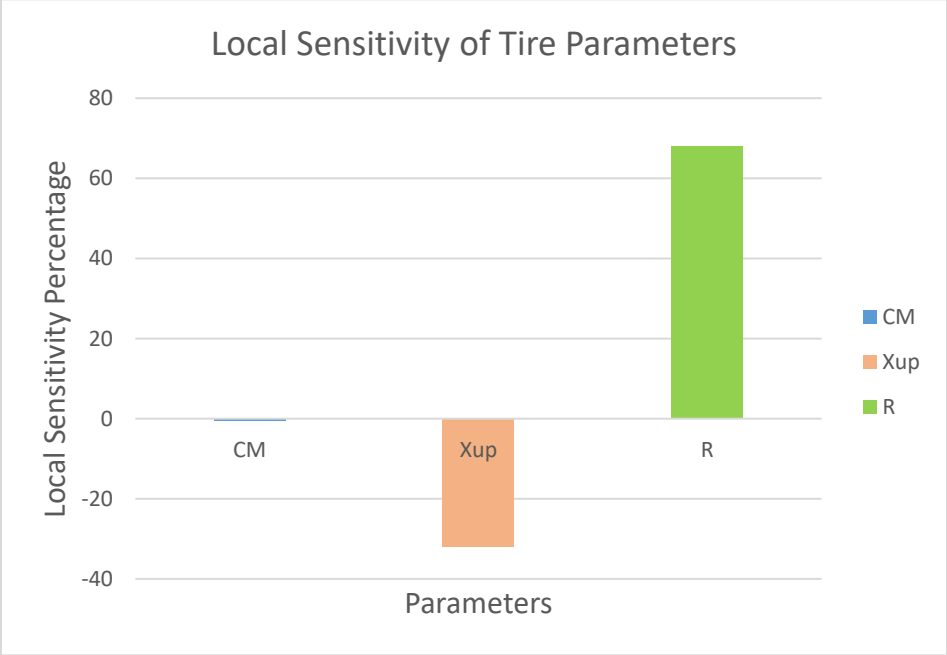

Figure 4-14: Local Sensitivity% for the three Parameters

Figure 4.14 shows the local sensitivity percentage of the three parameters, shoulder radius(R), and the side wall profile (CM and Xup). As seen, the local sensitivity percentage of the shoulder radius is 68% while the sensitivity percentage of CM is -0.6% and that of Xup is -32%. The sensitivity percentage was calculated in ANSYS Design Explorer using the response surface function and was plotted in Microsoft Excel. The parameters were set using the design of experiments component of ANSYS by specifying the range and the output parameter was set to drag area. From this plot, we can observe that the shoulder radius is the most sensitive parameter.

4.1.5 Further Discussion

We can now look at particular cases of interest from our parametric study. From our parametric study, we find the highest and lowest drag case as shown in Table 4.2.

Table 4-2: Tire Parameters for the Highest and the Lowest Drag Case

Case	R(mm)	Xup(mm)	CM(mm)	Drag Area(m^2)
Highest Drag	197.027	0.405405	190.2702	0.68
Lowest Drag	194.054	0.539191	196.9595	0.57

Figure 4-15: Tire Cross Sectional Profile for the Lowest Drag Case

Figure 4-16: Tire Cross Sectional Profile for the Highest Drag Case

Figures 4.15 and 4.16 represent the cross sectional profile of the tires for the highest and the lowest drag case. From the cross-sectional profiles, the lowest drag case has a much more streamlined profile than the highest drag case.

Further studies can be conducted with more parameters to facilitate for a more detailed analysis of the tire geometry. This would help further improve the tire design for drag performance optimization.

4.2 Rim Protector Sensitivity

In this section, the general flow past a rotating tire on the ground is discussed, the design of experiments based parametric sensitivity study results are discussed. A short discussion based on the Coefficient of pressure along the tire cross section is provided in order to understand the flow past an isolated tire.

The output parameter chosen for the sensitivity study to understand the impact of the rim protector parameters is the overall drag area of the tire model. The rim protector parameters are then ranked based on their drag area contribution.

4.2.1 Flow Features

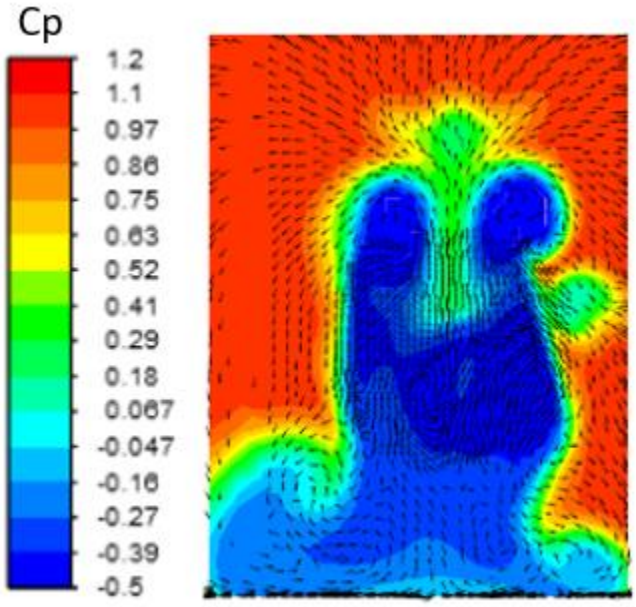

Figure 4-17: Total Pressure Coefficient Contour at the wake plane

Figure 4.17 shows the total coefficient of pressure contour with vectors at the wake plane directly behind the tire model. Figure 4.18 shows the wake plane coefficient of pressure distribution from experimental studies conducted by Schnepf *et al.* [14] The two plots showcase the total pressure

coefficient under different loading conditions and at different camber angles of the tire at the wake plane. It is observed that the two contours shown have a very similar structure to the contour plot found by our simulations. The vorticity of the flow at the wake plane can be seen developing on the left and right side of the tire.

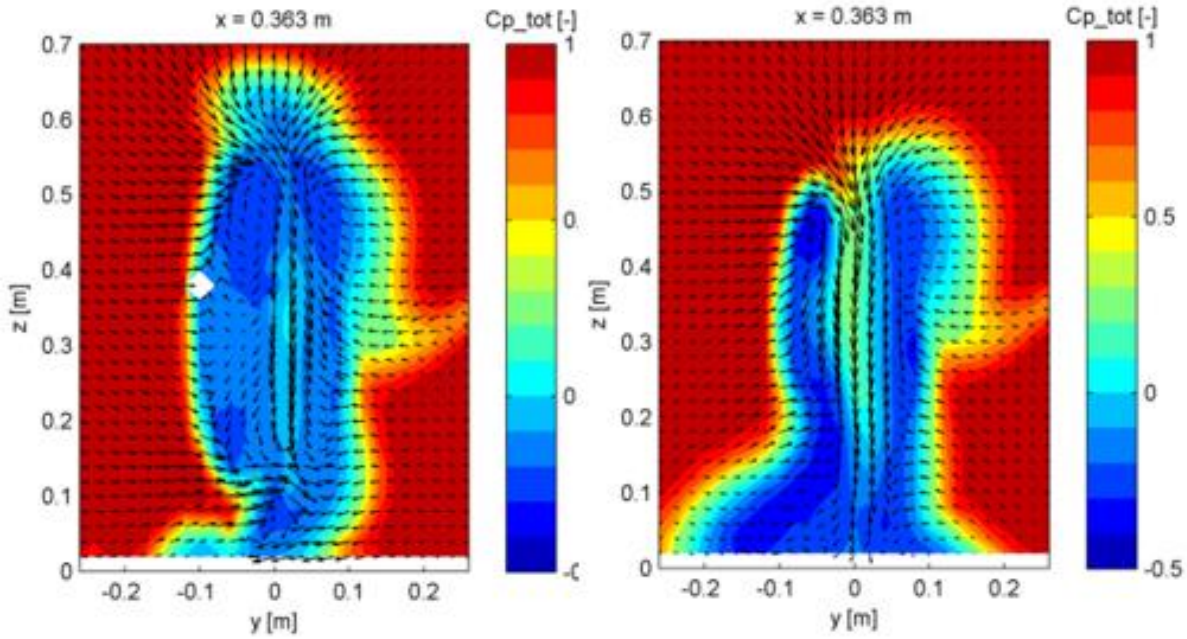

Figure 4-18: Left: Wake plane Total Cp with camber = 0.20 vertical load = 5300 N. Right: Wake plane Total Cp with camber = 0.250 vertical load = 5500 N [14]

This shows that our model can capture most of the flow characteristics around the tire and is adequate for our analysis.

4.2.2 The Parametric Study

The drag area was calculated for different configurations for the tire model using Design of Experiments. A design space was created given that 10 increments within the altitude range and 6 increments within the angle range were enough to capture the change in drag area sufficiently. Using this information, a 3D matrix was created consisting of all values of the three parameters and the Kennard-Stone algorithm [23,24] was used in order to create the design space. This design space was then used to calculate the drag area of the tire model for the various different parameter combinations.

It should be noted that in order to maintain the integrity of the triangle, the three parameters, the base angles and the altitude, cannot be truly independent. But if the constraints are defined such that the three parameters can change independently, we would rid ourselves of the need of having a perfect triangle for all the design points.

Design Of Experiments Regression Model

To validate the Kennard-Stone algorithm for further analysis, a linear regression study is conducted. The linear model used can be written as:

$$Drag\ Area = Intercept + (360 - Angle1) * A + (360 - Angle1) * A + (360 - Angle1) * A \quad 11$$

A linear regression model is used since the Kennard-Stone algorithm has been shown to demonstrably perform well with regression models such as the Partial Least Squares method [26].

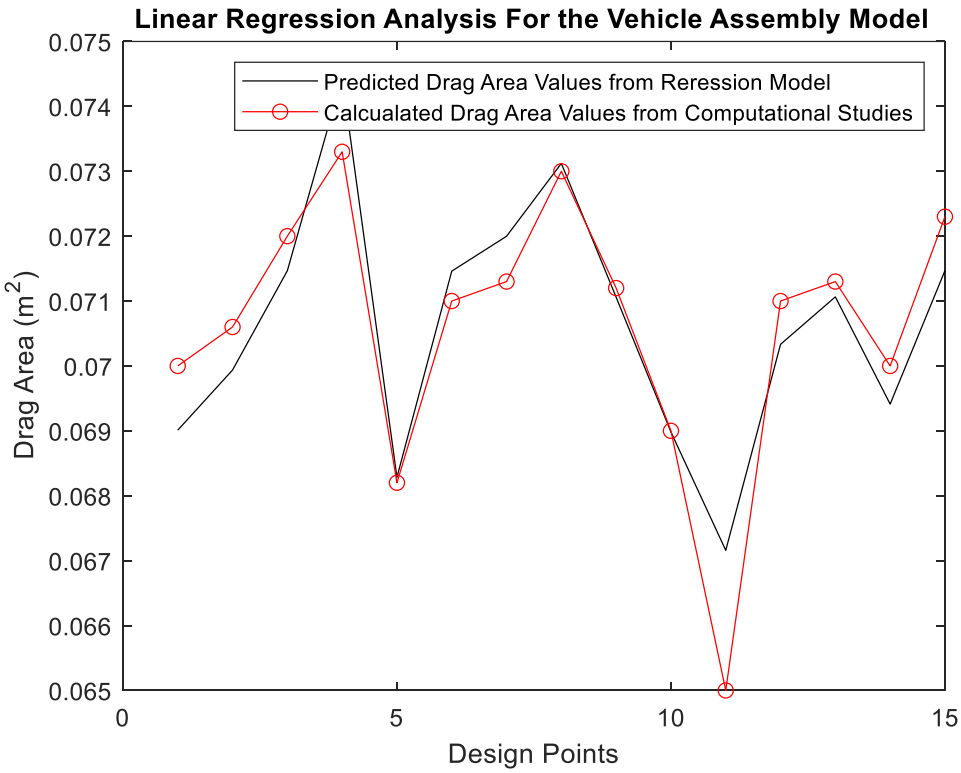

Figure 4-19: Comparison of Calculated Drag Area and Regression Predicted Drag Area

Figure 4-19 shows that the linear regression model is able to predict the drag area output with an

R^2 value of 0.834. The regression model was able to predict the drag area output with a p value of 0.0001339 which is sufficient for the model.

Table 0-3: Equation Coefficients from Regression Analysis

	Coefficients
Intercept	0.04621835
360-Angle 1	2.92697E-07
360 -Angle 2	8.95874E-05
Altitude	-0.000494549

Table 4-3 shows the intercept and the coefficients of the three parameters or the values A, B and C in equation 12.

Response Surfaces

Using the simulated drag area results, ASNYS Design Explorer was used to plot 2D response plots, 3D response surfaces and the local sensitivity percentage of the three parameters in order to determine the impact rank of the three parameters.

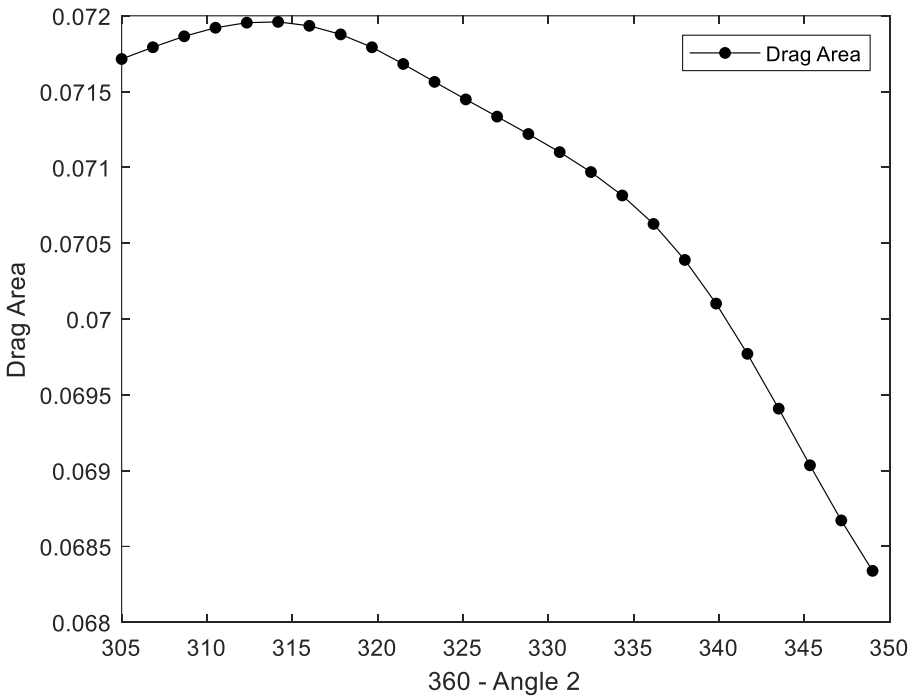

Figure 4-20: Impact of Angle 2 on the Drag Area

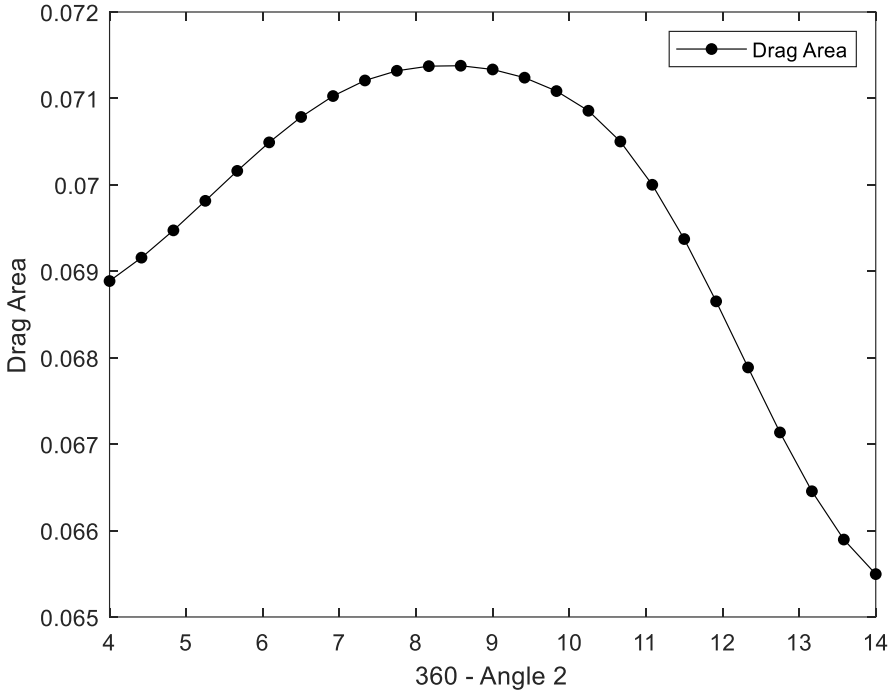

Figure 4-21: Impact of Altitude on the Drag Area

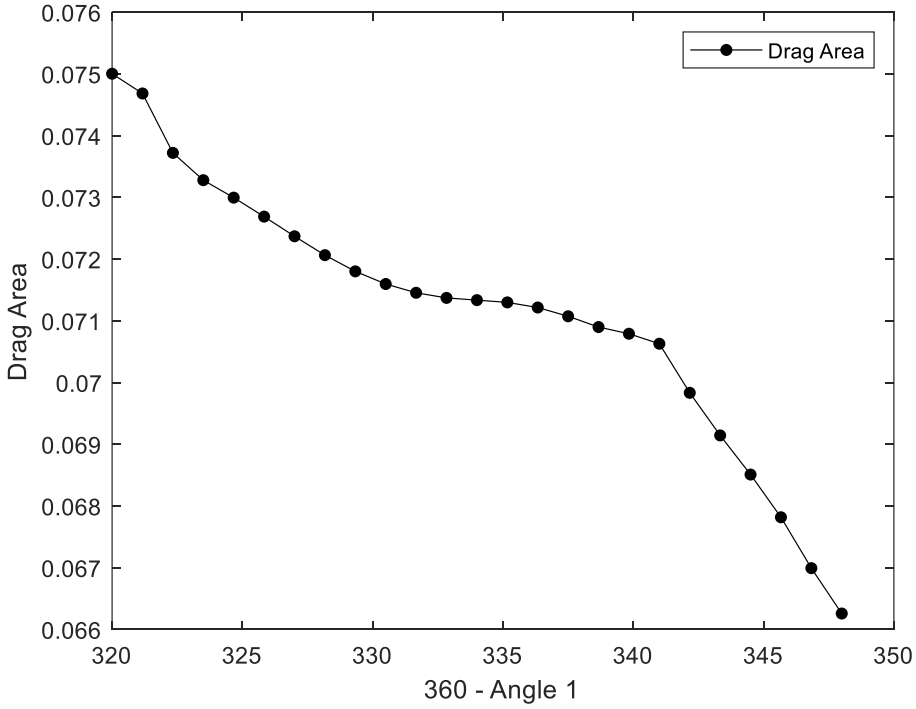

Figure 4-22: Impact of Angle 1 on the Drag Area

Figure 4.20 shows the impact of 360 - Angle 2 on the drag area of the tire model. The curve is

continuous with a very gradual slope. From Figure 4.21 the curve for the Altitude is steeper than 360 – Angle2. Whereas, from Figure 4.22, 360 – Angle 1 has the steepest slop and can affect the drag area the most.

These curves are, however, based on the regression analysis of the design space used for the study. In order to understand the linear regression model used to construct the response surfaces, we look at the goodness of fit curve shown in Figure 4.23.

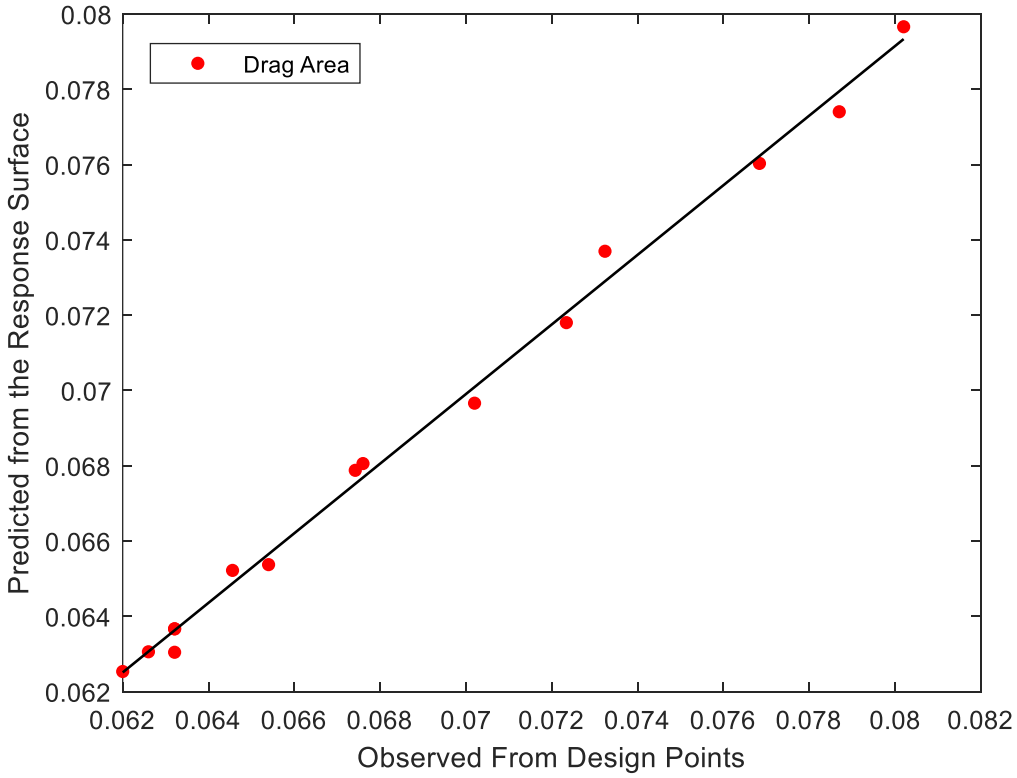

Figure 4-23: Goodness of Fit Curve

The R^2 value for this curve is 0.9926. From the goodness of fir curve, it can be seen that our regression model is pretty good for the representation of the parametric impact of the rim protector.

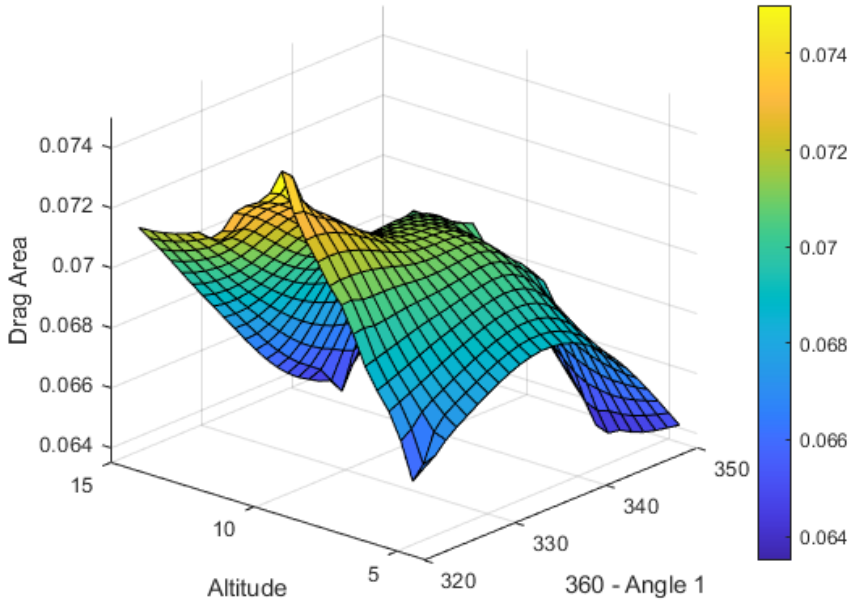

Figure 4-24: Response Surface Capturing the effect of Angle 1 and Altitude on the Drag Area

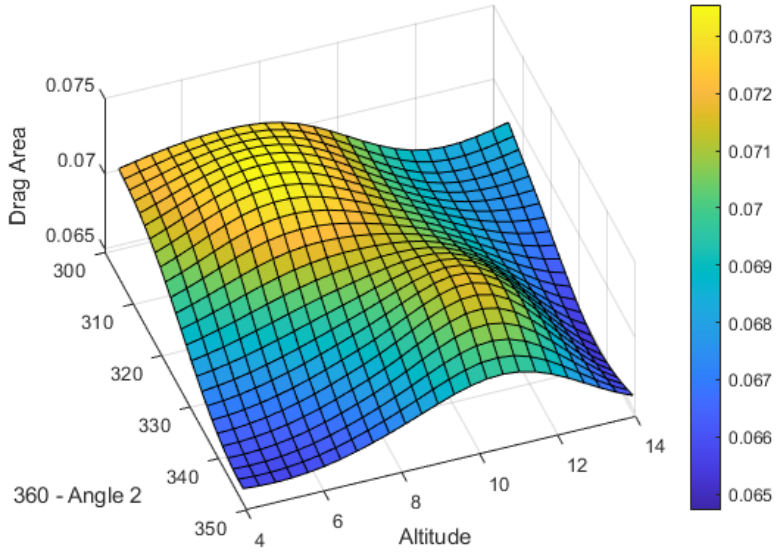

Figure 4-25: Response Surface Capturing the effect of Angle 2 and Altitude on the Drag Area

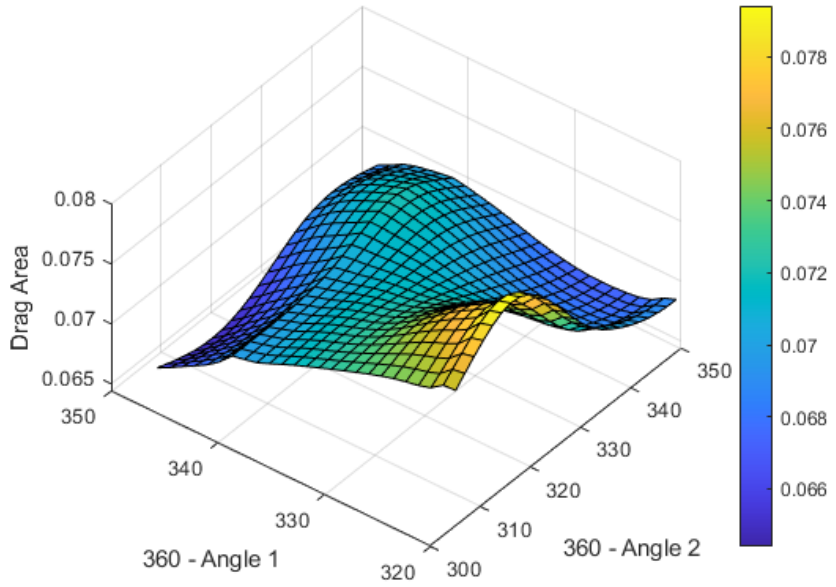

Figure 4-26: Response Surface Capturing the effect of Angle 1 and Angle 2 on the Drag Area

Figures 4.24, 4.25 and 4.26 show the 3D response surfaces based on the drag area output. From Figure 4.24, we can see that the impact of both Angle 1 and the altitude on the drag area are similar. While from figure 4.25 it is evident that the impact of the altitude is greater than the impact of Angle 2. Similarly, from Figure 4.26, it can be seen that the impact of Angle 2 on the drag area is lower than the impact of Angle 1.

While it might seem that angles 1 and 2 would have similar impact on the drag area, it is not the case. This is due to the fact that the 2 angles determine if the rim protector bulges from above or below. So it is important to note the difference in the impact of the two parameters for future studies.

Now, using the same tool, ANSYS Design Explorer, a local sensitivity plot was determined as shown in Figure 4.27.

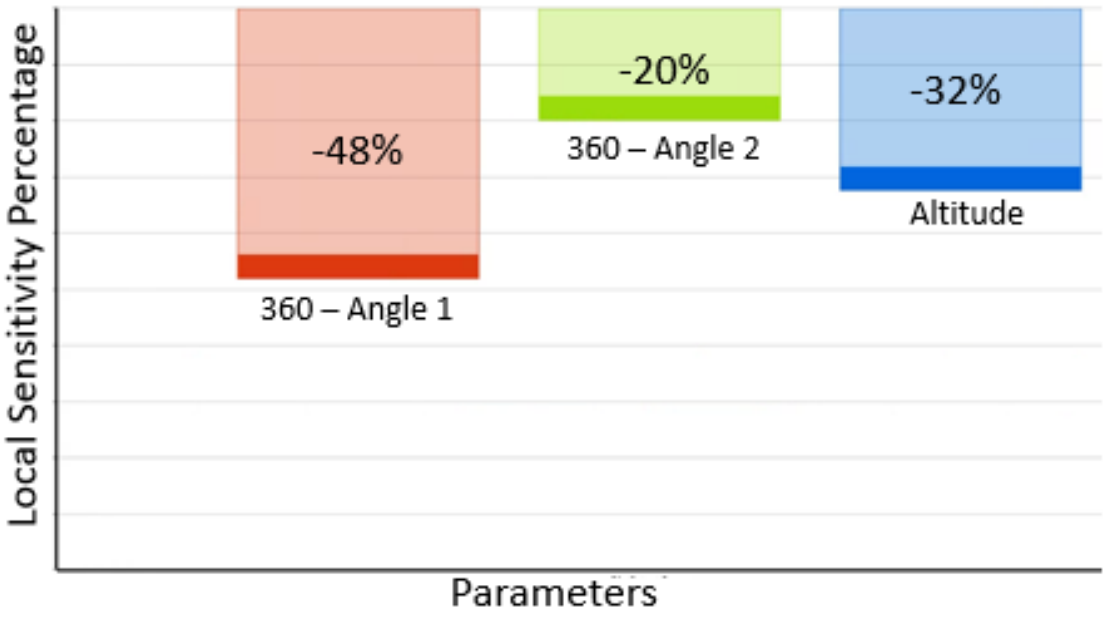

Figure 4-27: Local Sensitivity Plot

From this plot, we can see that Angle 1 is the most sensitive parameter, followed by Altitude and finally the least impactful parameter is Angle 2. Based on the response plots and surfaces, this result was to be expected.

4.2.3 Further Discussion

Table 4.4 shows the minimum and maximum drag cases for the rim protector.

Table 4-4: Highest and Lowest Drag Cases

Case	360 – Angle 1	360 – Angle 1	Altitude (mm)	Drag Area(m^2)
Lowest Drag	305.00	339.58	14	0.08
Highest Drag	320.55	319.73	9.02	0.10

From Table 4.4 the two particular cases of our parametric study can be useful to understand the

geometry of the rim protector at the maximum and minimum drag cases.

Further, more detailed, studies can be conducted on the parametric analysis of the rim protector. This could include more complex rim protector parameters with lesser concessions made for the sake of simplicity. Analysis can also be done on a Vehicle – Tire Assembly for more realistic results which depend on the geometry of the entire vehicle.

Chapter 5: Conclusions

The goal of this study was to parameterize the rim protector design on an isolated tire and parametrize the overall tire in a tire – vehicle assembly to conduct computational fluid dynamics simulations. This was done to conduct a sensitivity analysis of to find the impact rank of the parameters.

From this study, we were able to conclude that:

1) The impact rank of the three parameters for the tire cross section is, 1-Angle 1, 2-Altitude and 3-Angle 2.
2) The upward or downward bulge of the rim protector geometry can lead to very varied results in terms of the drag contribution of the tire. This is even if the degree of bulge is the same on both sides.
3) Of the three parameters based on the cross-section profile and the shoulder radius, the shoulder radius is the most sensitive.
4) The impact rank of the three parameters for the tire cross section is, 1-Shoulder Radius, 2-Xup and 3-CM. It was seen that variable CM has the lowest impact amongst all the parameters.

This study helps understand the drag contribution of one of the most important features of the tire and the rim protector. There are very few studies conducted on this particular component of the tire, but it nevertheless is a very important parameter to consider.

It is believed that the study conducted and discussed in this paper can be a good first step toward drag optimization by varying the tire geometry. For further studies, a more extensive and detailed parametric analysis can be undertaken for the optimization of the drag performance of the vehicle. In terms of the rim protector analysis, more complex rim protector parameters can be utilized. This can also be done on a Vehicle – Tire Assembly for more realistic results which depend on the geometry of the entire vehicle

References

[1]Hobeika, Teddy, and Simone Sebben. 2018. “Tyre Pattern Features and Their Effects on Passenger Vehicle Drag.” *Sae International Journal of Passenger Cars - Mechanical Systems* 11 (5): 401–13. https://doi.org/10.4271/2018-01-0710.

[2] Heft, Angelina I, Thomas Indinger, Nikolaus A Adams, and SAE 2012 World Congress & Exhibition Detroit, Michigan, United States 2012-04-24. 2012. “Introduction of a New Realistic Generic Car Model for Aerodynamic Investigations.” *Sae Technical Paper* (20120416).

[3] Axon, L., Garry, K., and Howell, J., 1998, "An Evaluation of CFD for Modelling the Flow Around Stationary and Rotating Isolated Wheels," SAE International.

[4] Leśniewicz, P., Kulak, M., and Karczewski, M., 2014, "Aerodynamic analysis of an isolated vehicle wheel," Journal of Physics: Conference Series, 530.

[5] Landström, C., Walker, T., Christoffersen, L., and Löfdahl, L., 2011, "Influences of Different Front and Rear Wheel Designs on Aerodynamic Drag of a Sedan Type Passenger Car," SAE Technical Paper Series.

[6] Landstrom, C., Josefsson, L., Walker, T., and Lofdahl, L., 2012, "Aerodynamic Effects of Different Tire Models on a Sedan Type Passenger Car," SAE International Journal of Passenger Cars - Mechanical Systems, 5(1), pp. 136-151.

[7] Landström, C., Josefsson, L., Walker, T., and Löfdahl, L., "An experimental investigation of wheel design parameters with respect to aerodynamic drag," Proc. FKFS Conference.

[8] Ashton, Neil, Alistair Revell, and SAE 2015 World Congress & Exhibition Detroit, Michigan, United States 2015-04-21. 2015. “Comparison of Rans and Des Methods for the Drivaer Automotive Body.” *Sae Technical Paper* (20150414). https://doi.org/10.4271/2015-01-1538.

[9] Ashton, N, A West, S Lardeau, and A Revell. 2016. “Assessment of Rans and Des Methods for Realistic Automotive Models.” *Computers and Fluids* 128: 1–15.

[10] Soares, Renan F, Kevin P Garry, Jennifer Holt, and WCX™ 17: SAE World Congress Experience Detroit, Michigan, United States 2017-04-04. 2017. “Comparison of the Far-Field Aerodynamic Wake Development for Three Drivaer Model Configurations Using a Cost-Effective Rans Simulation.” *Sae Technical Paper* (20170328). https://doi.org/10.4271/2017-01-1514.

[11] Soares, Renan Francisco, de Souza Francisco José, and 24th SAE Brasil International Congress and Display Sao Paulo, Brazil 2015-09-22. 2015. “Influence of Cfd Setup and Brief Analysis of Flow Over a 3d Realistic Car Model.” *Sae Technical Paper* (20150922). https://doi.org/10.4271/2015-36-0513.

[12] Reiß, J., Sebald, J., Haag, L., Zander, V. et al., “Experimental and Numerical Investigations on Isolated, Treaded and Rotating Car Wheels,” SAE Technical Paper 2020-01-0686, 2020, doi:10.4271/2020-01-0686.

[13] Heo, H., Ju, J., Kim, D., and Kim, H., "A Computational Study of the Flow Around an Isolated Non-Pneumatic Tire,"*SAE Int. J. Passeng. Cars - Mech. Syst.* 7(1):2014, doi:10.4271/2014-01-9123.

[14] Schnepf, B., Schütz, T., and Indinger, T., "Further Investigations on the Flow Around a Rotating, Isolated Wheel with Detailed Tread Pattern," *SAE Int. J. Passeng. Cars - Mech. Syst.* 8(1):2015, doi:10.4271/2015-01-1554.

[15] Zhou, Haichao, Zhen Jiang, Guolin Wang, and Shupei Zhang. 2021. “Aerodynamic Characteristics of Isolated Loaded Tires with Different Tread Patterns: Experiment and Simulation.” *Chinese Journal of Mechanical Engineering* 34 (1). https://doi.org/10.1186/s10033-020-00528-1.

[16] Misar, A.S., Uddin, M., Robinson, A., and Fu, C., “Numerical Analysis of Flow around an Isolated Rotating Wheel Using a Sliding Mesh Technique,” SAE Technical Paper 2020-01-0675, 2020, doi:10.4271/2020-01-0675.

[17] Kurachi, Sena, Hideyuki Kawamata, Kenichi Hirose, Shuji Suzuki, Munehiko Oshima, and WCX SAE World Congress Experience Detroit, Michigan, United States 2020-04-21. 2020. “Aerodynamic Sensitivity Analysis of Tire Shape Factors.” Sae Technical Paper (20200414). https://doi.org/10.4271/2020-01-0669.

[18] Fu, G, & Untaroiu, A. "Effects of Tire Attributes on Aerodynamic Performance." *Proceedings of the ASME 2020 International Mechanical Engineering Congress and Exposition. Volume 10: Fluids Engineering*. Virtual, Online. November 16–19, 2020. V010T10A033. ASME. https://doi.org/10.1115/IMECE2020-24615

[19] Fu, Gen, and Alexandrina Untaroiu. 2021. “Investigation of Tire Rotating Modeling

Techniques Using Computational Fluid Dynamics." *Journal of Fluids Engineering* 143 (11). https://doi.org/10.1115/1.4051311.

[20] Collin, Christopher, Steffen Mack, Thomas Indinger, Joerg Mueller, and SAE 2016 World Congress and Exhibition Detroit, Michigan, United States 2016-04-12. 2016. "A Numerical and Experimental Evaluation of Open Jet Wind Tunnel Interferences Using the Drivaer Reference Model." *Sae International Journal of Passenger Cars - Mechanical Systems* 9 (2): 657–79. https://doi.org/10.4271/2016-01-1597.

[21] Mercker, E., Wickern, G., and Weidemann, J., "Contemplation of Nozzle Blockage in Open Jet Wind-Tunnels in View of Different 'Q' Determination Techniques," SAE Technical Paper 970136, 1997, doi:10.4271/970136.

[22] Young, A., Squire, H., "Blockage correction in a closed rectangular tunnel," ARC, R.&M. 1984, 1945

[23] R.W. Kennard, L.A. Stone, Computer aided design of experiments, Technometrics 11 (1969) 137-148

[24] M. Daszykowski, B. Walczak, D.L. Massart, Representative subset selection, Analytica Chimica Acta 468 (2002) 91-103

[25] Schnepf, B. H., 2016, "Untersuchung von Einflussfaktoren auf die Umströmung eines PKW-Rades in Simulation und Experiment," Technische Universität München.

[26] Ferreira, Roberta de Amorim, Gabriely Teixeira, and Luiz Alexandre Peternelli. 2022. "Kennard-Stone Method Outperforms the Random Sampling in the Selection of Calibration Samples in Snps and Nir Data." *Ciência Rural* 52 (5). https://doi.org/10.1590/0103-8478cr20201072.